NUMERICAL SIMULATION OF INITIAL VELOCITY/DISPLACEMENT CONDITIONS IN A DYNAMIC CENTRIFUGE TEST

S P G Madabhushi

CUED/D-Soils TR237 1990

NUMERICAL SIMULATION OF INITIAL VELOCITY/DIPLACEMENT CONDITIONS IN A DYNAMIC CENTRIFUGE TEST

Madabhushi.S.P.G *

Abstract: In numerical simulation of dynamic centrifuge model tests, use of correct initial conditions is important. A mathematical approach which can be used to determine the initial velocity/displacement conditions from any given digitised acceleration signal was presented together with a step by step scheme. The proposed scheme was evaluated using the base accelerations of six centrifuge model earthquakes. In each case the scheme was able to predict the initial conditions satisfactorily.

Using these initial conditions a centrifuge model test RSS111 was analysed using a finite element code. For all the six model earthquakes of this centrifuge test the results from the numerical analysis agreed with the centrifuge test data when correct initial conditions were used. One analysis with zero initial conditions resulted in unsymmetric pore pressure generation and movement of the structure in the horizontal direction, emphasizing the need for use of correct initial condtions in the numerical analyses.

1 Introduction

Centrifuge modelling has provided deep insight into complex geotechnical problems. Use of centrifuge modelling to simulate dynamic problems in Soil Mechanics has been established over last decade at the Cambridge University, Schofield (1981). The dynamic test data obtained has been used by many research workers to validate the Finite Element programs developed recently, Habibian (1987), Venter (1987), Jeyatharan (1989), Madabhushi (1989). The common approach used by all the researchers was to use a Finite Element program to analyse any given centrifuge test and compare the results of the numerical experiment with the actual centrifuge test results. A finite element mesh representing the centrifuge model is prepared and the base nodes of the mesh are subjected to actual acceleration observed at the base of the model during the dynamic centrifuge test. Many of the researchers have used zero initial velocity and displacement conditions. However such conditions introduce a shift in the velocity term and cause the drift of the displacement term due to the inherent integration procedure involved.

Assume a simple sinusoidal accleration

* Research Student,Cambridge University Eng. Department, Trumpington Street, Cambridge, CB2 1PZ, U.K.

$$a(t) = a_0 \, Sin(\omega t) \tag{1}$$

By integrating

$$v(t) = -\frac{a_0}{\omega} Cos(\omega t) + C_1 \tag{2}$$

and

$$d(t) = -\frac{a_0}{\omega^2} Sin(\omega t) + C_1 t + C_2 \tag{3}$$

If v(0)=0 and d(0)=0 then

$$v(t) = -\frac{a_0}{\omega} Cos(\omega t) + \frac{a_0}{\omega} \quad 'shift - term' \tag{4}$$

$$d(t) = -\frac{a_0}{\omega^2} Sin(\omega t) + \frac{a_0}{\omega} t \quad 'drift - term' \tag{5}$$

In this paper, the effect of the initial velocity and displacement conditions on the numerical integration and hence on the whole analysis are studied. A new mathematical approach was considered to compute the appropriate initial velocity and displacement conditions and a step by step scheme was presented to bring about these computations. The scheme was then used in conjunction with a finite element program 'Swandyne', Chan (1988), to analyse a centrifuge model test RSS111, Steedman (1986).

2 Review of literature

Biot (1956) has presented governing equations for the behaviour of a porus medium saturated with fluid treating them as a coupled system. Many modifications have been made to the Biot's equations since then. Chan (1988) has listed many of the modifications and has incorporated them into his unified program SWANDYNE which uses a staggered displacement-pore pressure (u-p) formulation. If the finite element solution for the Biot's equations are considered for the case of dynamic loading (undrained condtion) one can write

$$[M]\,\ddot{u} + [K]\,u - [Q]\,p = \bar{f} \tag{6}$$

$$[Q]^T \ddot{u} + [S]\dot{p} + [H]p \quad = \quad \bar{f} \tag{7}$$

where [M] - Mass matrix

[K] - Stiffness matrix

[Q] - Coupling matrix of the two phases

[S] - Compressibility matrix

[H] - Permeability matrix

u - displacement of solid phase

p - pore pressure of fluid phase

The scheme starts by using the steady state pore pressures and solves the Eq. 6 to get the displacements which are then substituted in Eq. 7 to compute the modified pore pressures. Thus the coupled system is solved in a staggered fashion. After solving these equations at any time 't', the time marching is brought forward by using finite differences schemes for the numerical integration. For the present purpose Generalised Newmark (2nd order interpolation for the 2nd order polynomial) GN22 scheme was used. If the acceleration time history is known then the velocity/displacement can be obtained as

$$\dot{u}_{t+1} \quad = \quad \dot{u}_t + \ddot{u}_t\,(1-\theta_1)\,dt + \ddot{u}_{t+1}\,\theta_1\,dt \tag{8}$$

$$u_{t+1} = u_t + \dot{u}_t\,dt + \ddot{u}_t\,(1-\theta_2)\,\frac{dt^2}{2} + \ddot{u}_{t+1}\,\theta_2\,\frac{dt^2}{2} \tag{9}$$

where θ_1 and θ_2 are constants and 'dt' is the data point spacing of the digitised acceleration signal. Using Eq. 8 and 9 the velocity and displacement time histories can be obtained provided the initial velocity and displacements are known.

In the next section a mathematical approach is suggested to compute these initial velocity and displacement for a given centrifuge test whose input acceleration is available in the digitised form. These initial conditions are then used to perform the numerical integration using Eq 8 and 9.

In order to compute the discrete fourier transform of the digitised acceleration signal the algorithm suggested by Cooley etal (1969) was used. This algorithm splits the given time series into sub-series until each of these will have only one term. Then the fourier transform of the single term series is computed as

$$X_k = \sum_{k=1}^{k=\infty} x_k \, e^{\frac{-2\pi kt}{T}} \tag{10}$$

and these components are then reassembled to give the fourier transform of the original time series. This procedure requires $N \, Log_2 N$ computations to evaluate the transform, where N is the number of data points in the series. Also the algorithm requires that this number N must be a power of 2.

3 Formulation

A typical accleration trace obtained from a centrifuge test can be considered as a periodic signal if the time window is long enough, as the trace can then be assumed to repeat itself outside the window. Now any signal that is periodic can be represented as

$$a(t) = a_0 + 2 \sum_{k=0}^{k=\infty} a_k \, cos \frac{2\pi kt}{T} + 2 \sum_{k=1}^{k=\infty} b_k \, sin \frac{2\pi kt}{T} \tag{32 ~~11~~}$$

If the average acceleration is zero then a_0 vanishes and

$$a(t) = 2 \sum_{k=0}^{k=\infty} a_k \, cos \, \omega_k \, t + 2 \sum_{k=1}^{k=\infty} b_k \, sin \, \omega_k \, t \tag{33 ~~12~~}$$

$$where \quad \omega_k = \frac{2\pi k}{T} \tag{34 ~~13~~}$$

By integration, velocity

$$v(t) = 2 \sum_{k=1}^{k=\infty} \frac{a_k}{\omega_k} \, sin \, \omega_k \, t + 2 \sum_{k=0}^{k=\infty} \frac{-b_k}{\omega_k} \, cos \, \omega_k \, t + C_1 \tag{35 ~~14~~}$$

Now if the initial velocity were to be

$$v(0) = -2 \sum_{k=0}^{k=\infty} \frac{b_k}{\omega_k} \qquad (\cancel{15})\ 36$$

the constant C_1 vanishes.

Now the displacement is obtained by integrating the velocity

$$d(t) = -2 \sum_{k=0}^{k=\infty} \frac{a_k}{\omega_k^2} \cos \omega_k t - 2 \sum_{k=1}^{k=\infty} \frac{b_k}{\omega_k^2} \sin \omega_k t + C_2 \qquad (\cancel{16})\ 37$$

By similar arguement the initial displacement is

$$d(0) = -2 \sum_{k=0}^{k=\infty} \frac{a_k}{\omega_k^2} \qquad (\cancel{17})\ 38$$

so that C_2 is zero.

Thus by computing the initial velocity and displacement using Eq. 14 and 16 , the shift term and drift term of Eq. 4 and 5 can be eliminated.

However, it should be possible to compute the initial velocity/displacement conditons from the mechanics of the bumpy road excitation system used to generate the input acceleration, Kutter(1982). It should be noted that such a value would only be of limited use as before each earthquake such a value might change due lack of mechanical fit of the excitation system. Also the solution scheme is very sensitive to the initial conditions as demonstrated in Section 5.0.

4 Proposed scheme

The mathematical approach developed in the last section can be implemented using the following scheme.

step i) compute the average acceleration. Offset the acceleration trace by the average. This ensures that a_0 term of Eq. ~~11~~ 7.32 is zero.

step ii) Compute the Discrete Fourier Transform of the trace

$$A(N) \xrightarrow{DFT} a_k + i\, b_k \qquad (18)$$

step iii) Filter the low frequencies and high frequencies using a band pass filter. Effects of bandwidth are investigated in the next section.

step iv) Reconstruct the acceleration trace by performing a IDFT and compare the filtered trace with original trace.

step v) Compute the initial velocity and displacement by evaluating the summations in Eq. ~~14~~ 7.35 and ~~16.~~ 7.36.

step vi) Using these initial conditions perform the numerical integration using a GN22 scheme as shown in Eq. ~~8~~ 7.25 and ~~9.~~ 7.26

Compare the acceleration, velocity and displacement traces.

The advantage of the procedure is that it involves computing the discrete fourier transform of the base acceleration trace and the initial velocity/displacement only once before the actual F.E. analysis is started. These conditions will then ensure the accuracy of the integration procedure during the time stepping in the actual analysis as explained in Sec. 2.0.

5 Numerical evaluation of the scheme

5.1 Sensitivity

In order to test the sensitivity of the GNpj integration scheme to the initial velocity and accleration conditions a numerical experiment was carried out using a sinusoidal signal of the form

$$a(t) = 100\, sin(240\, t) \tag{19}$$

According to Eq. 14 the initial velocity must be $\frac{100}{240\pi} = 0.1326291$. The numerical integaration was performed using the above value as v(0) and later by altering this value by a mere 15 percent (0.1127347) and the results are presented in Fig. 5.1 and Fig. 5.2. Clearly in Fig 5.2 the displacement is effected by the drift term and increases with time while in Fig. 5.1 it oscillates with the same frequency as the acceleration. (with 180^0 phase shift).

5.2 Base accleration of a centrifuge model

The base acceleration from a typical centrifuge model RSS111, Earthquake 1 was filtered to remove the very low and very high frequencies. As explained in Sec. 4.0, the initial velocity/displacement were computed and the numerical integration was performed. In Fig. 5.3 the original trace together with the filtered trace and the velocity and displacement traces obtained by the numerical integration are presented. In Fig. 5.4 the spectral analyses of the same trace are presented before and after the filtering process. In order to check the stability of the the proposed scheme several other base acceleration traces for Earthquakes 2 to 6 were analysed and the results are shown in Figures 5.5 through 5.9. In each case it was found that satisfactory displacement traces which do not under go drift with time could be obtained using this scheme.

5.3 Band Pass Filter

In the proposed scheme the necessity to filter the very low frequencies was identified. Using the base acceleration observed during Earthquake 1 for this centrifuge model the effects of the bandwidth of the filter on the integration scheme were studied. The numerical integration itself would reduce the high frequencies to certain extent (as it involves division with the square of the frequency while computing the displacement term). Comparing Fig. 5.10 and Fig 5.12 it is evident that the low frequencies need to be filtered as when the low frequencies are present the displacement trace oscillates with this low frequency. However, sufficient care must be excercised in choosing the lower cut off frequecy of the filter so that none of the dominant modes of vibration of either the structure or the soil column are eliminated. For this, a preliminary fourier analysis of acceleration traces at various transducer positions in the centrifuge model can be carried out to find the dominant modes of vibration.

6 Analysis of the centrifuge test RSS111

Centrifuge test RSS111 was a dynamic test in which a solid structure was embedded into a sand embankment. The sand embankment was saturated using silicone oil of viscocity 80 cs to scale the permeability effects accurately, Schofield (1981). Details of the materials used in the construction of the model and the method of construction

can be obtained from the data report, Steedman (1986).

The section of the model is shown in Fig. 6.1 along with the positioning of the transducers within the model. The section of the model was discretised as shown in Fig. 6.2 into 35 elements using 8 noded quadrilateral elements and 6 noded triangular elements. The structure was assumed to be rigid during the analysis. The positions at which the output was obtained during the numerical analyses which correspond to the positions of the transducers in the centrifuge model are shown in Fig. 6.3. Six earthquakes were fired on the model during the centrifuge test using the bumpy road excitation system, Kutter (1982). The soil-structure system was analysed for each earthquake using the finite element code 'SWANDYNE', Chan (1988).

6.1 Earthquake 1

The acceleration observed at the base of the model during the centrifuge test was processed as explained in Sec. 5.2. This acceleration was then used as the input acceleration at all of the base nodes of the F.E. grid shown in Sec. 2.0. The initial velocity and displacement conditions obtained by the proposed scheme were applied at all of the base nodes.

6.1.1 Comparison of the results

The output obtained from the numerical analyses at homologus points were compared with the experimental data. In Figures 6.4 and 6.6 the time histories of acceleration, pore pressure and displacements at various points shown in Fig. 6.1 are plotted. The results from the numerical analyses are shown in Figures 6.5 and 6.7. In all the figures the accelerations are shown in the units of m/s^2 , excess pore pressures in the units of KPa and the displacements in metres.

The numerical analyses could predict the general trend of the accelerations, pore pressures and displacements observed during the actual centrifuge test. The magnitude of accelerations obtained from the F.E. analyses were satisfactory. The vertical accelerations shown at ACC 1925 and 1572 have high frequency components in both the centrifuge test and the numerical analyses. Smoothing of the acceleration trace as the shear wave travels up through the sand medium could be simulated in both centrifuge and numerical models as observed at ACC 3478 and ACC 3466.

The excess pore pressure histories obtained from the numerical analyses are comparable to the excess pore pressures generated during the centrifuge test. The shape of the pore pressure history at PPT 2842 (located at mid depth in sand) compares with the predicted pore pressure trace during the numerical analysis. The magnitudes of excess pore pressures observed in the experiment are lower compared to the values predicted by the F.E. analyses. The bimodality of frequency present in the pore pressure traces PPT 2631 and 2338 could be predicted during the first few cycles of the earthquake after which it was superposed by higher frequency components. It is important to note that the pore pressure traces at PPT 2855,2846 and PPT 2631,2338 which are symmetrically placed about the vertical axis, exhibit a 180° out of phase relationship with each other as in the case of the centrifuge test. The negative pore pressure observed at PPT 1111 as a result of the suction generated by rocking of the structure could be simulated by the numerical code.

The displacement traces of LVDT's 1648 and 4457 compare well with the observed experimental traces and have the same order of magnitude.

6.1.2 Pore pressure contours

From the numerical analysis pore pressure contours with a contour intervel of 10 KPa were plotted. In Fig. 6.8 these total pore pressure contours are shown after every 18.75 milliseconds. As the earthquake vibrations start the hydrostatic distribution of the pore pressures is altered due to generation of the excess pore pressures. The regions under the structure were subjected to large pore pressure rises. After the completion of the shaking the pore pressure distribution reaches a symmetric pattern.

The excess pore pressure contours are also shown at an intervel of 10 KPa in Fig. 6.9. The triangular marks indicate the regions of high excess pore pressures. The excess pore pressure contours confirm in the regions under the structure high excess pore pressures were generated. The pore pressure reach a symmetric pattern towards the end of the shaking and will dissipate with passage of time there after.

6.1.3 Analysis with zero initial conditions

In order to compare the influence of the initial conditions the analysis was repeated using zero initial velocity and displacements at the base nodes. The results from this analysis are presented in Fig. 6.10 . It is interesting to note that the pore pressure at

points symmetrically placed about the vertical axis of the model (PPT 2855 and 2856 ; PPT 2631 and 2338) no longer exhibit the 180° out of phase relationship. Also the horizontal displacement shown by LVDT 4457 increases with time as explained in Sec. 5.0. The rate at which the pore pressure is generated was different from the actual centrifuge experiment.

6.2 Earthquake 2

The base acceleration observed during the second earthquake was processed as explained in Sec. 5.2. Using this as the input acceleration and obtaining the initial velocity and displacement condtions the F.E. analysis was carried out.

The results from the centrifuge experiment are shown in Fig. 6.11 and 6.13 while those from the numerical analyses are presented in Fig. 6.12 and 6.14. As in the case of Earthquake 1 the numerical analysis compared reasonably well with the actual centrifuge test. However, it was interesting to note that the excess pore pressures generated during Earthquake 2 of the centrifuge test where lower than those in Earthquake 1. This tendency cannot be predicted by the numerical analyses as in each case the analysis would start from the same stress state of the soil while the actual sand in the centrifuge test would undergo some densification after each earthquake.

6.3 Earthquakes 3 to 6

Each of the earthquakes were processed as explained in Sec. 5.2 and the initial conditions were computed using the procedure explained earlier. The results from the centrifuge tests and the numerical analysis are presented in figures 6.15 through 6.30. The numerical analyses were comparable to the experimental data though it must be stressed that the F.E. analyses tend to give a band of solutions rather than the exact solution itself.

7 Conclusions

It is possible to evaluate the initial velocity and displacement of a given digitised acceleration signal using a discrete fourier transform. These initial conditions are important in the numerical integration schemes used by the Finite element programs,

especially when a centrifuge model test is being simulated using the numerical code. A systematic procedure was evolved to compute the initial conditions for any given trace. The procedure was evaluated using six different model earthquakes and it was found to yield satisfactory results in each case.

Using the correct initial conditions the finite element analyses were carried out for the centrifuge model test RSS111. For all the six model earthquakes analysed, the results from the numerical code compare favourably with the centrifuge test data. It was demonstrated that use of correct initial condtions is important in the numerical simulation of the dynamic centrifuge model tests.

ACKNOWLEDGEMENTS

The author wishes to acknowledge the motivation and guidence provided by Prof. Andrew Schofield during this work. He also wishes to acknowledge gratefully the help received from Dr.R.S.Steedman who provided with the data from the centrifuge experiments and was a sourse of constant inspiration at various stages of this work. Also the the constructive critisism by Dr.Richard Dean has been of immense help during every part of this work. The cooperation and friendly suggestions extended by Dr.Andrew Chan are gratefully acknowledged.

References

[1] Biot,M.A,(1956), Theory and propagation of elastic waves in fluid-saturated porus solid,Part I- Low frequency range, Part II- High frequency range , Jnl. of Acoustical Society of America, Vol. 28.

[2] Chan,A.H.C.,(1988), A unified finite element solution to static and dynamic problems of Geomechanics ,Ph.D Thesis, University college of swansea,Swansea.

[3] Chan A.H.C., User Manual for DIANA SWANDYNE-II , Institute for Numerical Methods in Engineering, University College of Swansea, 1988, also, Department of Civil Engineering, University of Glasgow, 1989.

[4] Cooley,J.W., Lewis,P.A.W. and Welch,P.D., (1969), The fast fourier transform and its applications , IEEE Transactions, Vol.12, No.1.,pp 27-34.

[5] Jeyatharan, K.,(1989), Private communications.

[6] Habibian, A., (1987), Seismic modelling of coastal dykes on layered sand foundations , Ph.D Thesis, Cambridge University.

[7] Hine, N.W., (1985), Starting conditions and procedures for solution of a 1-D

dynamic bar problem using SS22 and Newmark integation methods , C/R/530/85, University college of Swansea, Swansea.

[8] Kutter, B.L.,(1982), Centrifugal modelling of the response of clay embankments to earthquakes , Ph.D Thesis, Cambridge University.

[9] Schofield, A.N., (1981), Dynamic and Earthquake geotechnical centrifuge modelling , Int. Conf. on Recent Advances in Geotechnical Engineering and Soil Dynamics, Missouri, U.S.A.

[10] Steedman,R.S., Madabhushi,S.P.G. and Chan,A.H.C.,(1989), Numerical modelling of soils under dynamic loading , Int. Conf. on Engg. Software, New Delhi.

[11] Steedman,R.S., (1986), Embedded structure on sand foundation , Data Report on centrifuge, RSS110 and RSS111, C.U.E.D.

[12] Newland, D.,(1975), An introduction to Random vibrations and Spectral analysis , Longman Publishers., London.

[13] Robert, R.A. and Mullis,C.T., (1987), Digital signal processing , Wesley Publishers, London.

[14] Venter,K.V.,(1987), Modelling the behaviour of response of sand to cyclic loads , Ph.D Thesis, Cambridge University.

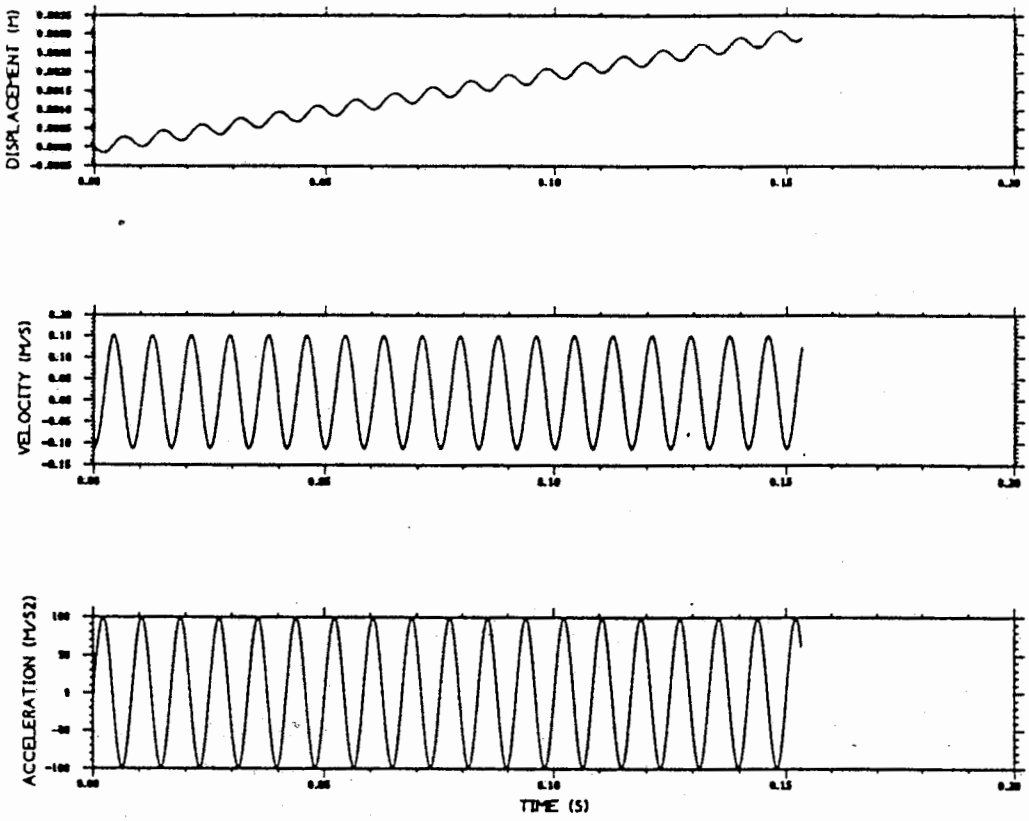

Fig. 5.2 Effect of Initiail conditions on integration (with 15 percent error)

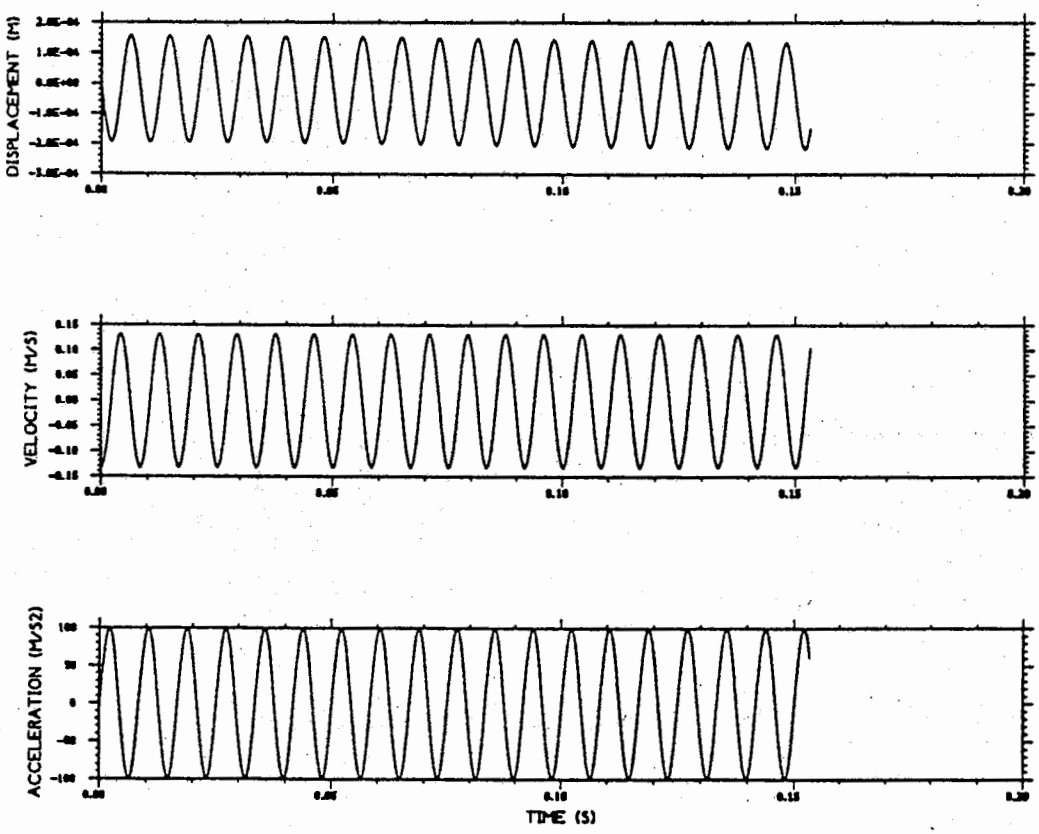

Fig. 5.1 Effect of Initiail conditions on integration (exact initial condition)

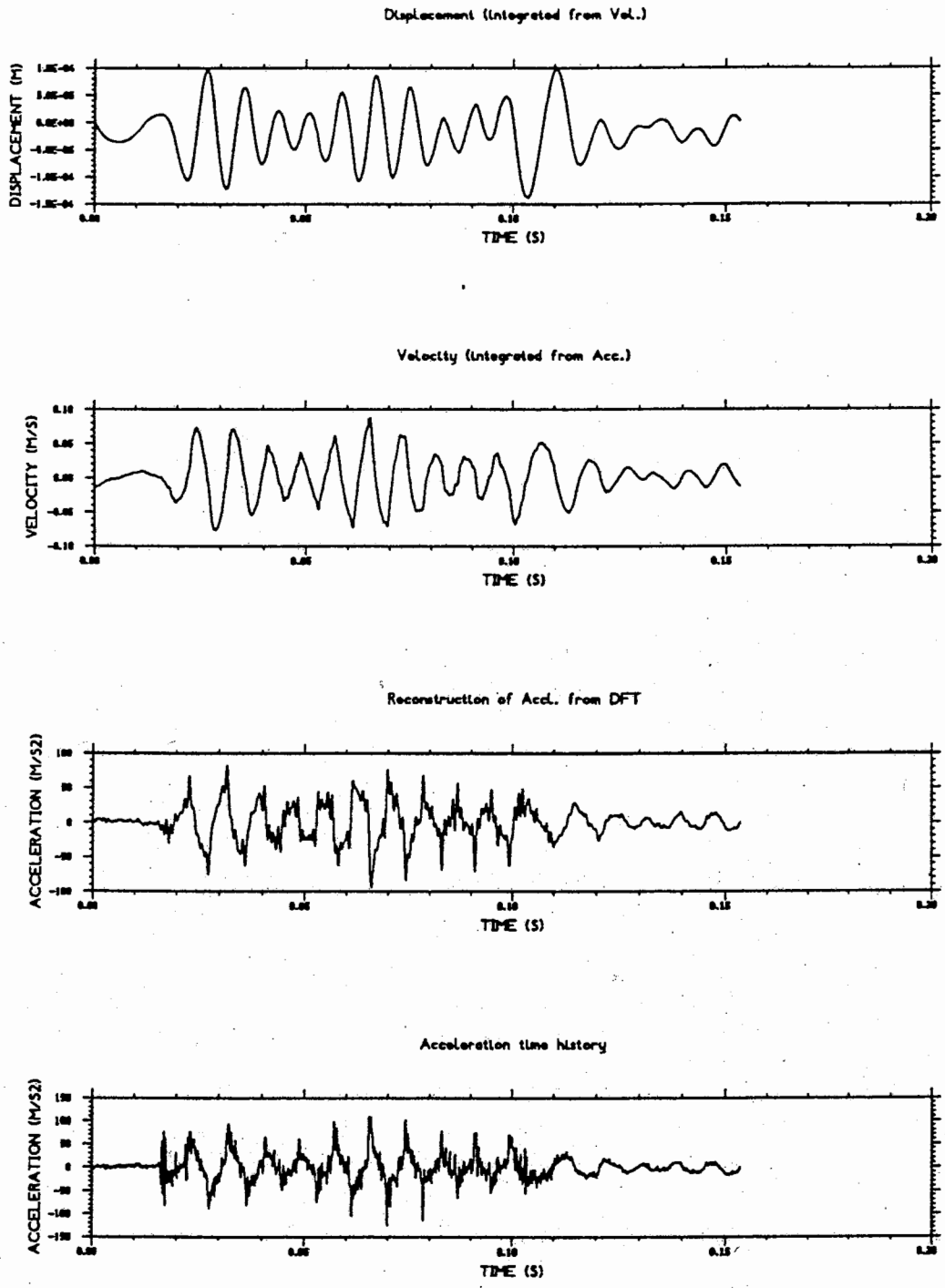

Fig. 5.3 Numerical Integration of base acceleration - EQ. NO:1 (Test RSS111)

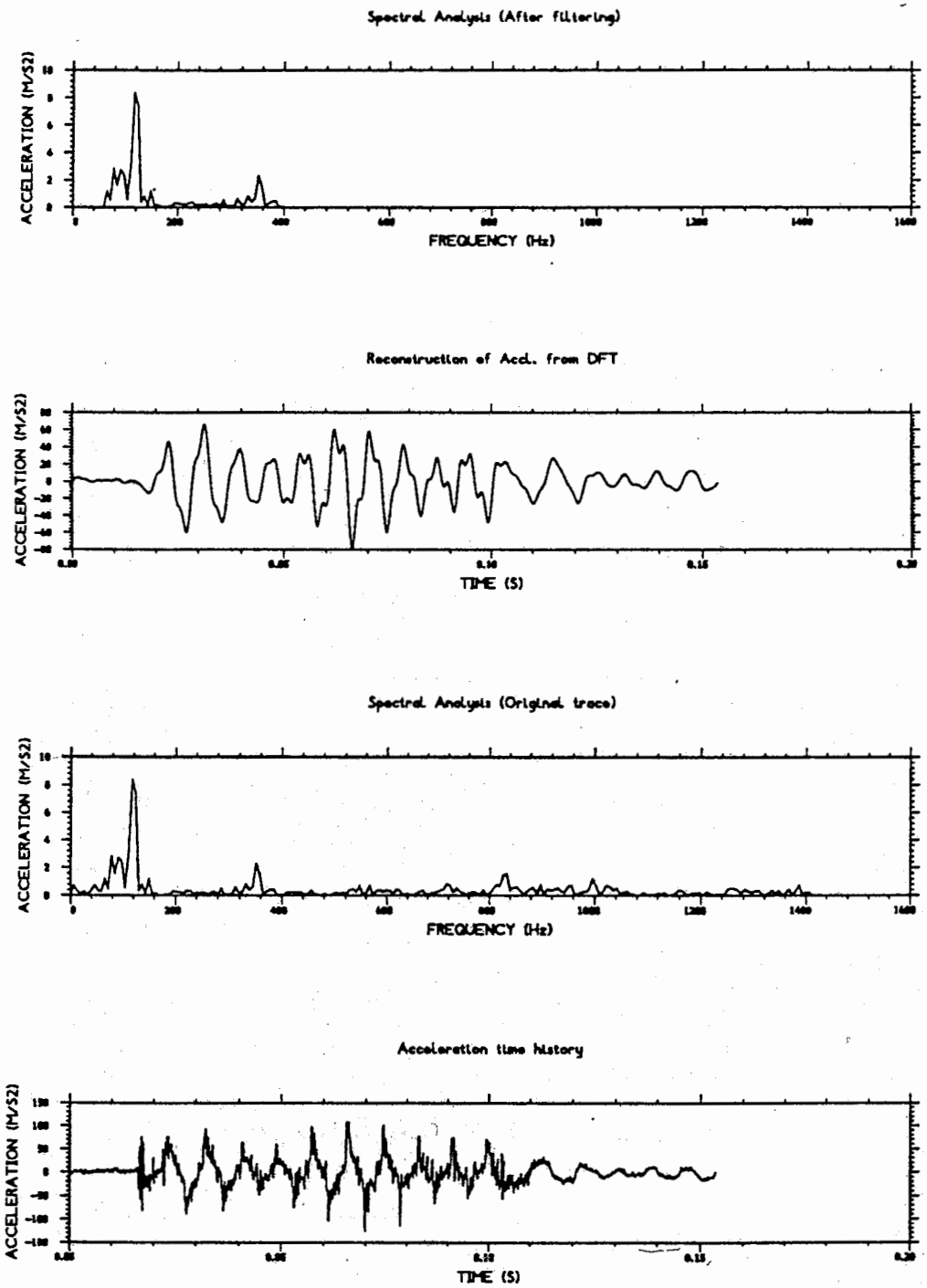

Fig. 5.4 Spectral Analysis for acceleration trace - EQ. NO:1 (Test RSS111)

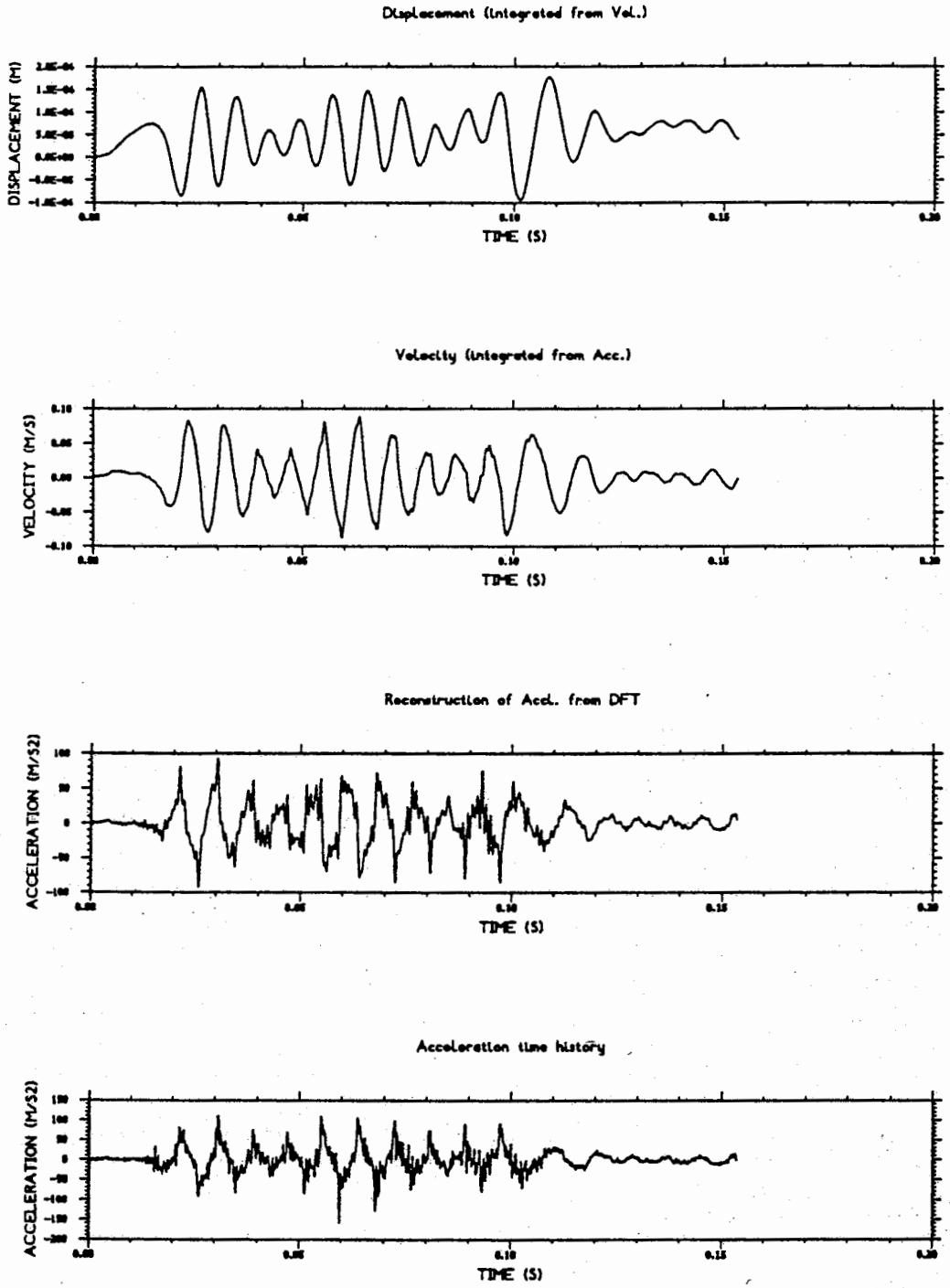

Fig. 5.5 Numerical Integration of base acceleration - EQ. NO:2 (Test RSS111)

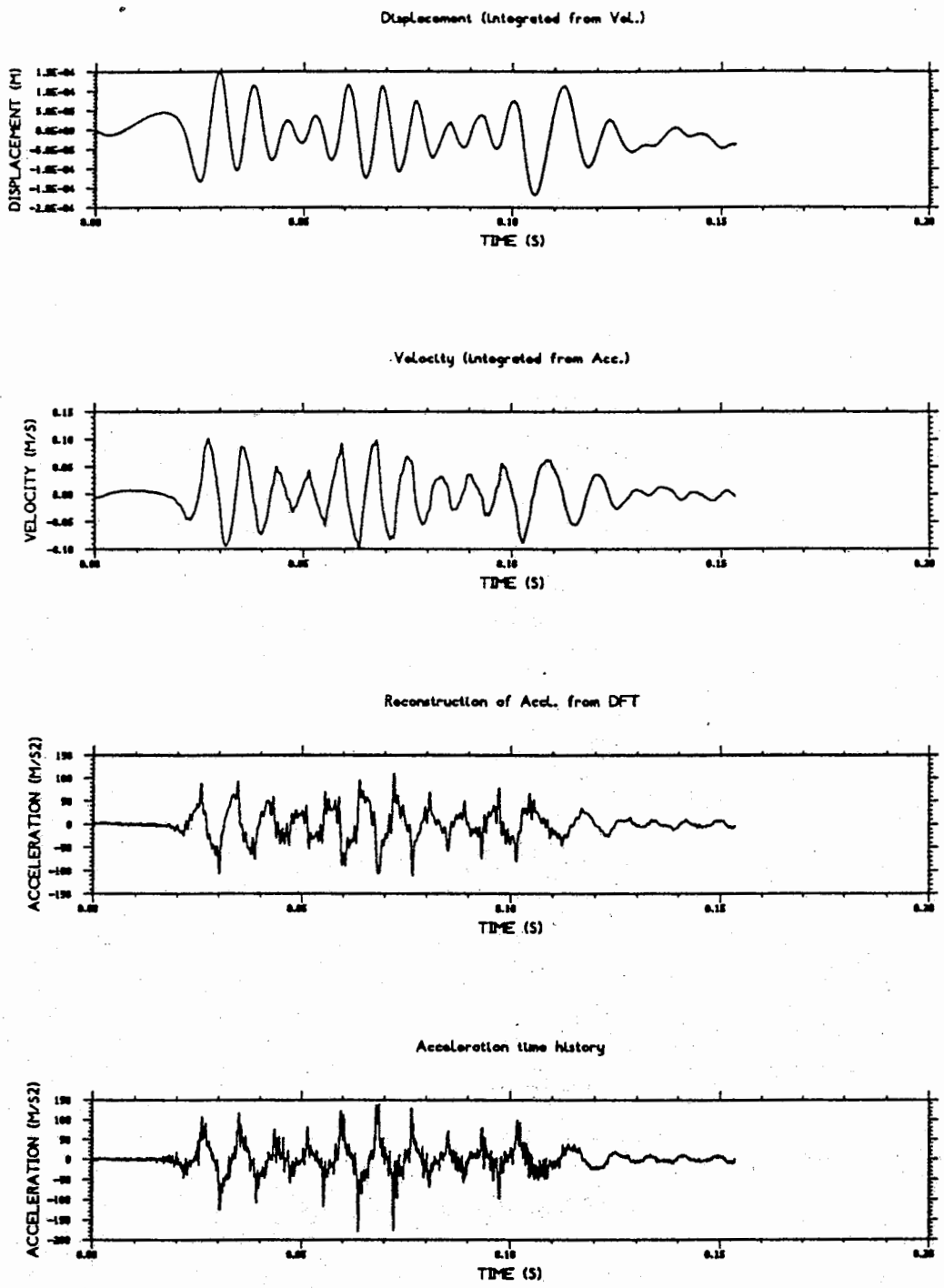

Fig. 5.6 Numerical Integration of base acceleration - EQ. NO:3 (Test RSS111)

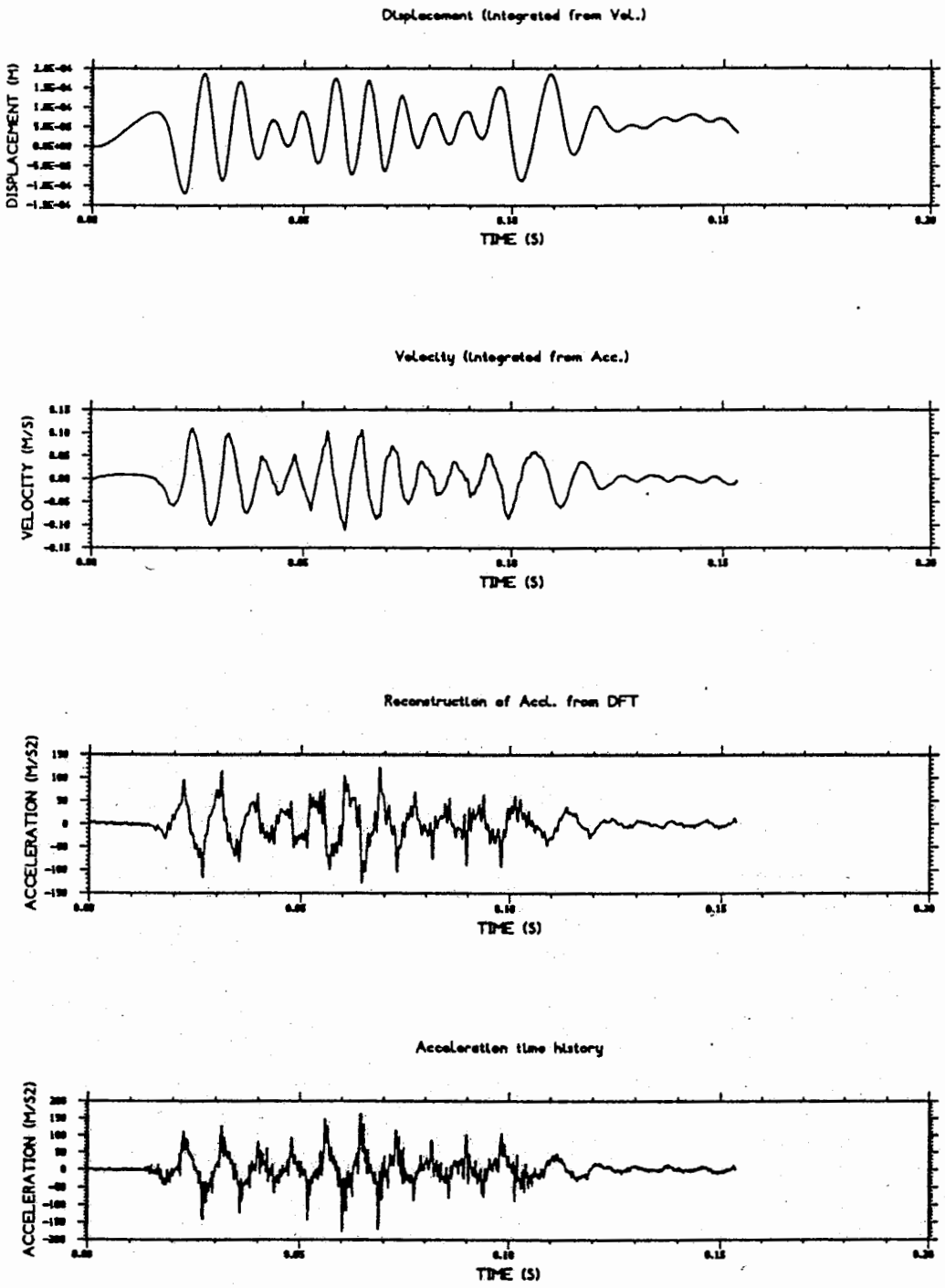

Fig. 5.7 Numerical Integration of base acceleration - EQ. NO:4 (Test RSS111)

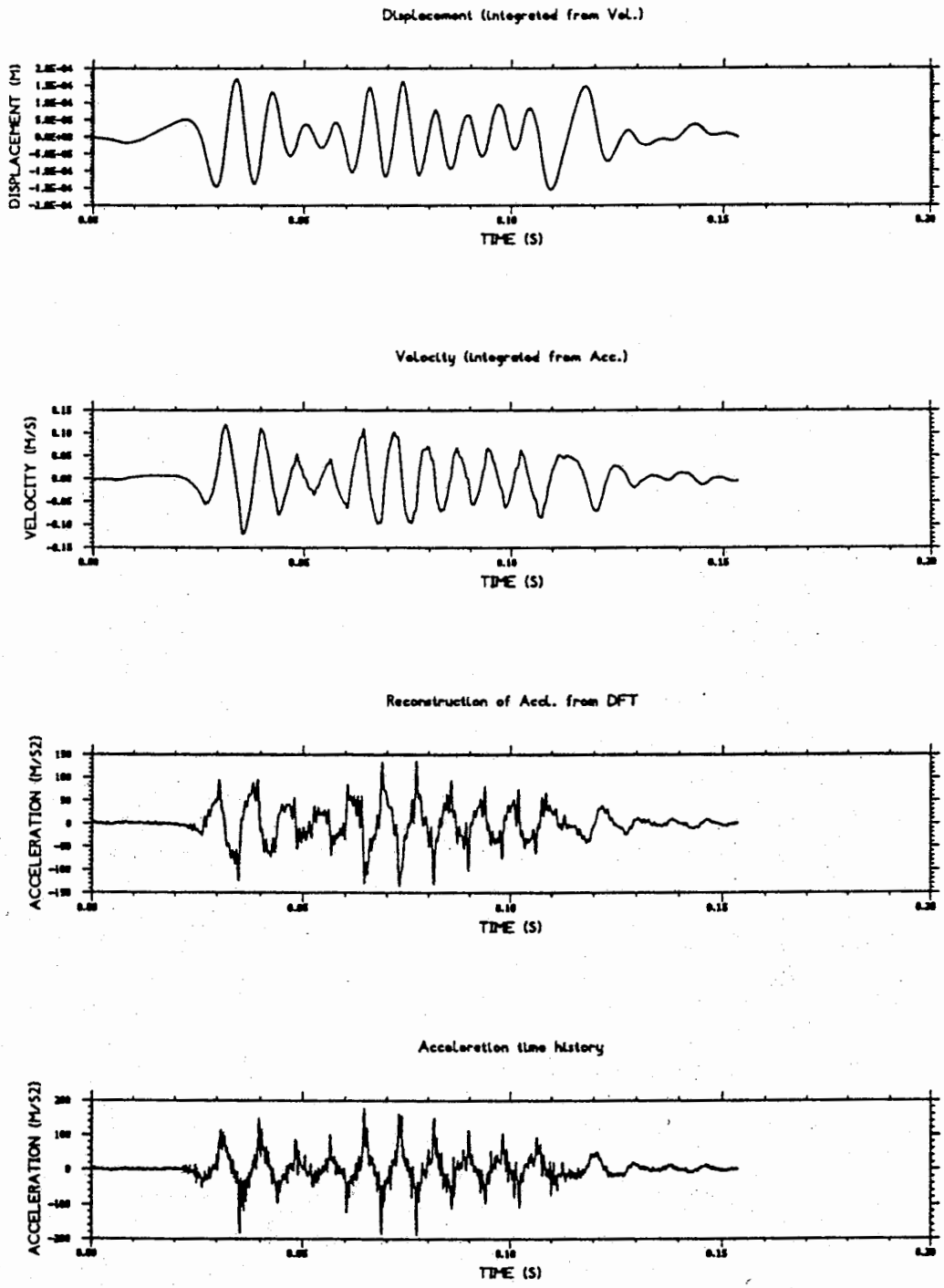

Fig. 5.8 Numerical Integration of base acceleration - EQ. NO:5 (Test RSS111)

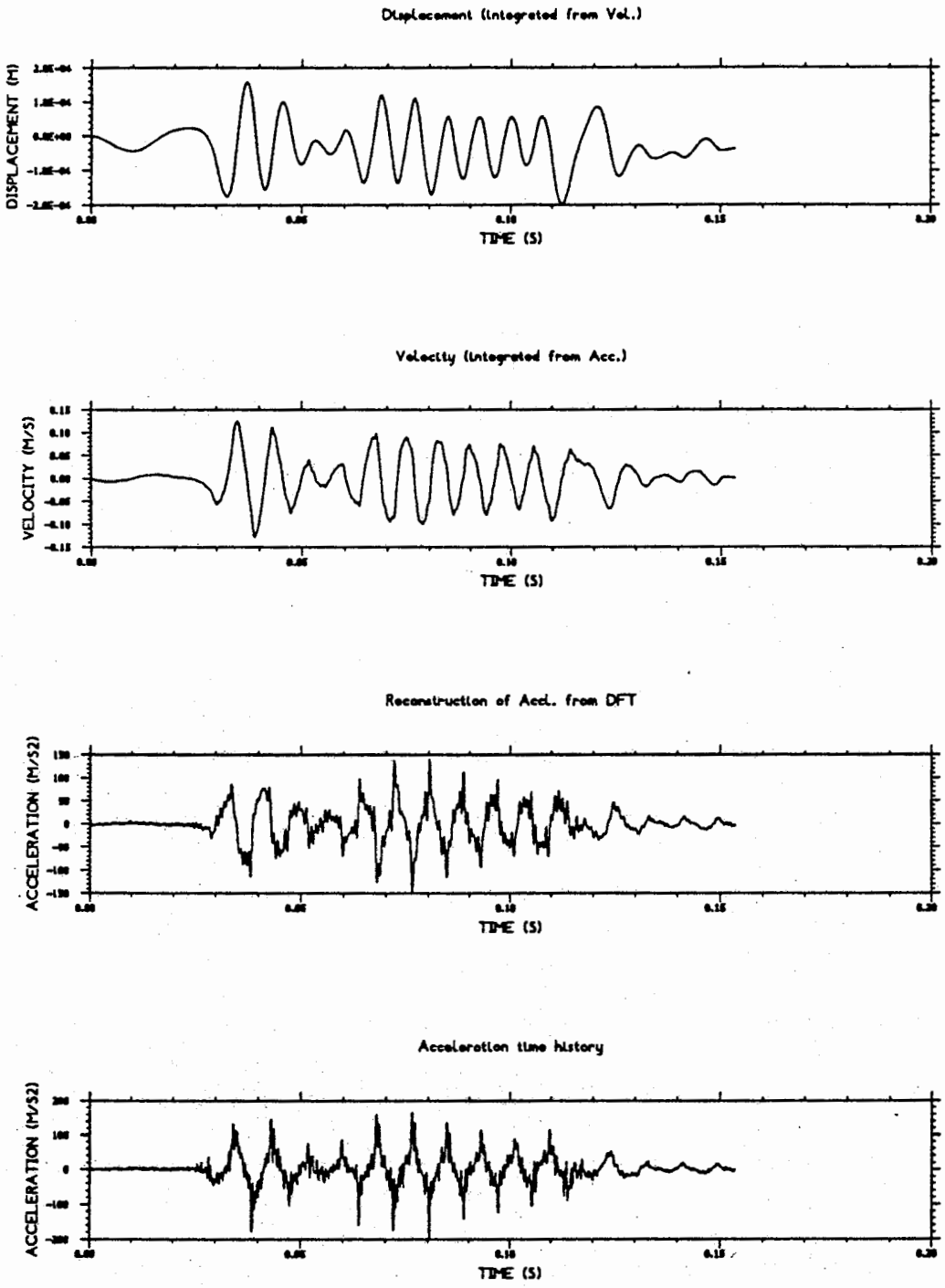

Fig. 5.9 Numerical Integration of base acceleration - EQ. NO:6 (Test RSS111)

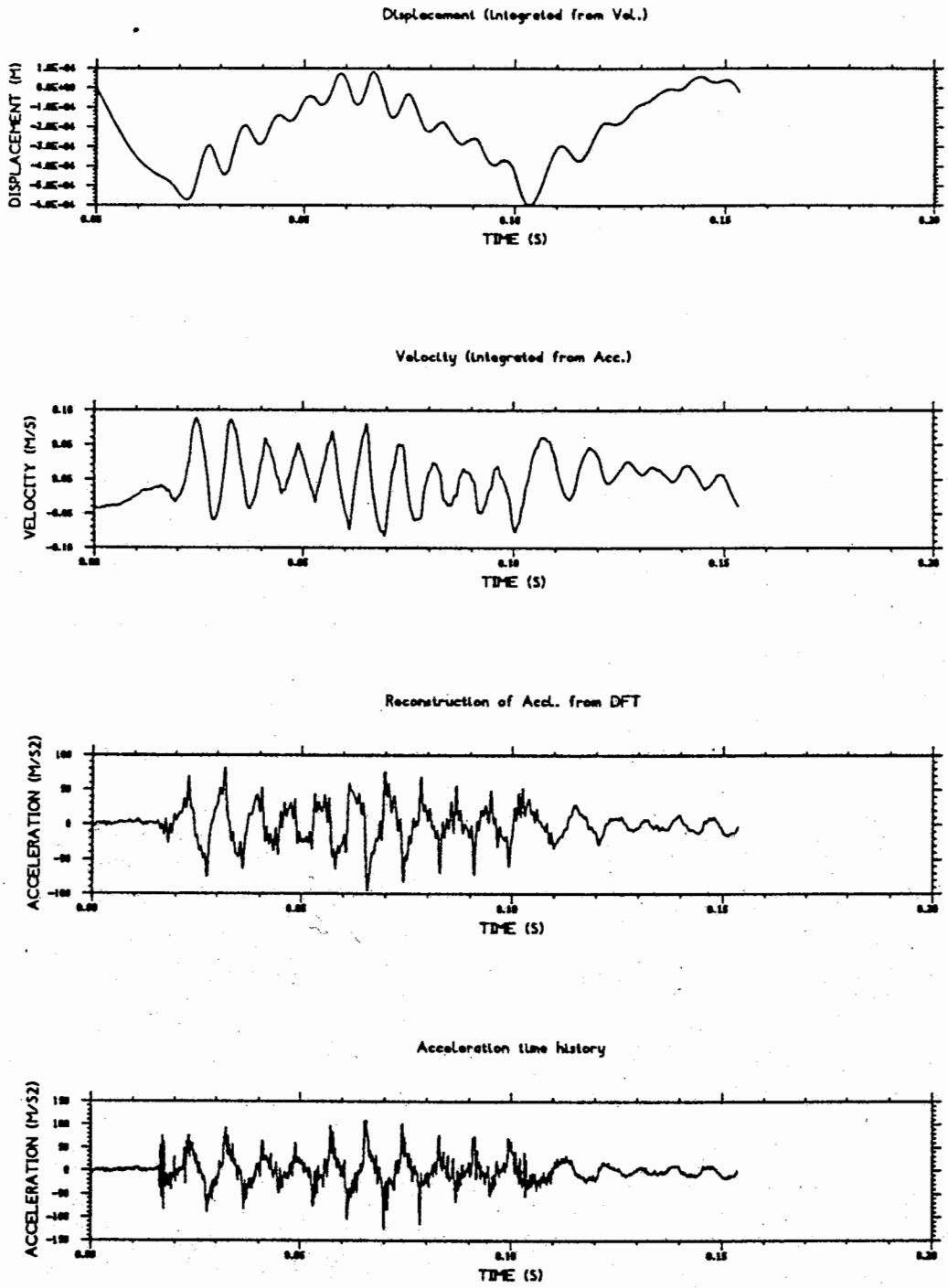

Fig. 5.10 Effects of Band width on numerical integration (0 hz to 1200 hz)

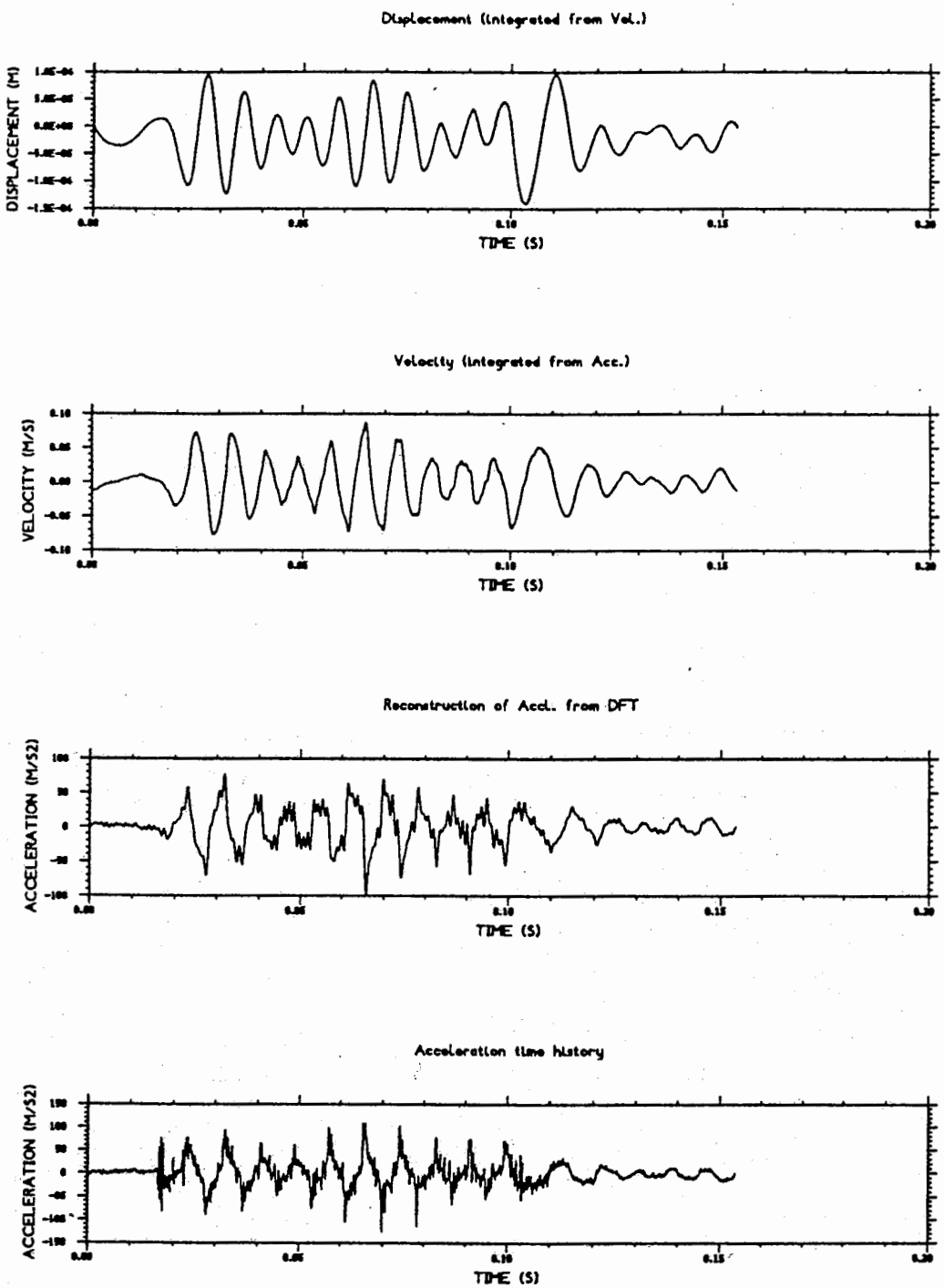

Fig. 5.11 Effects of Band width on numerical integration (30 hz to 900 hz)

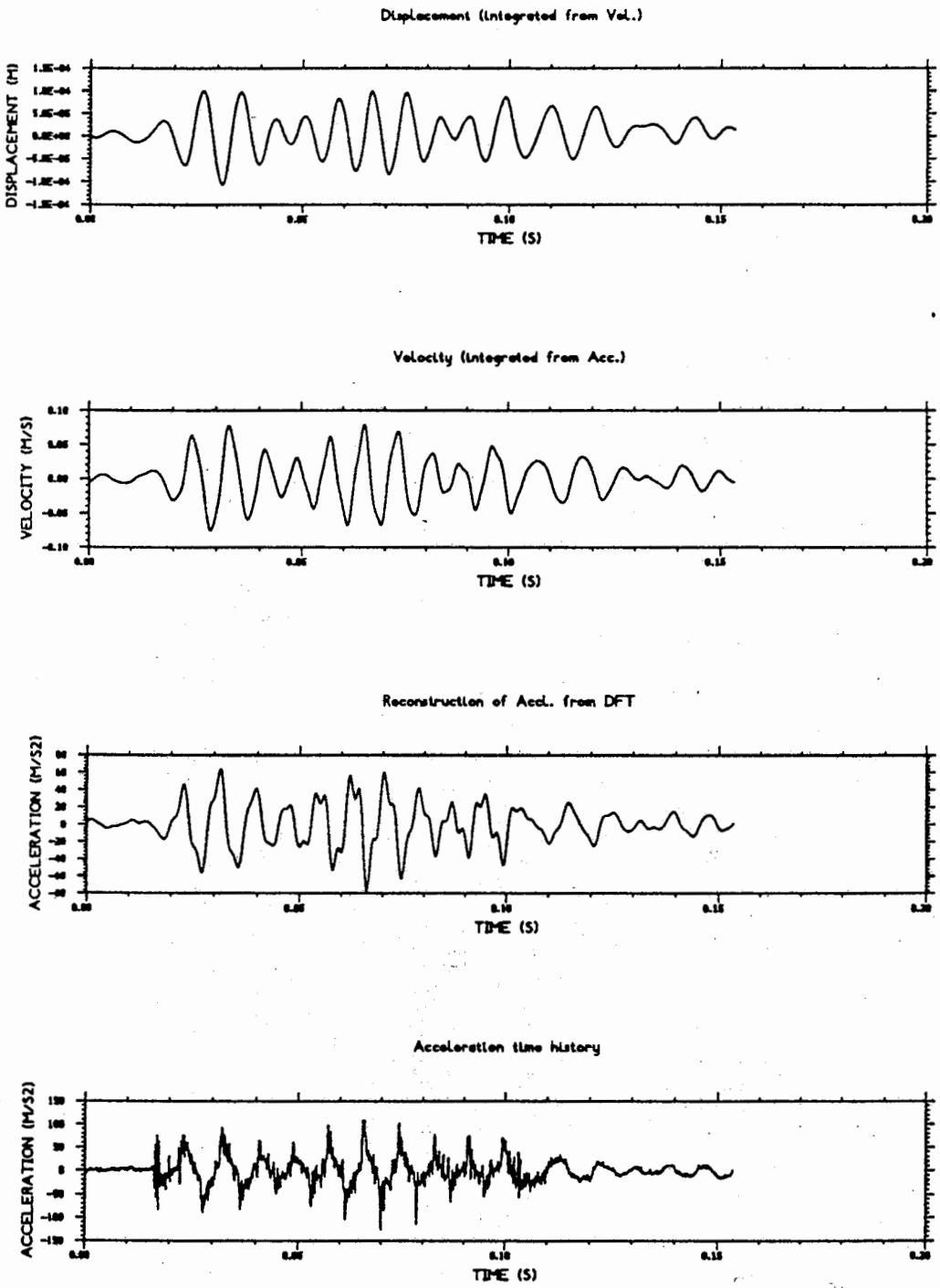

Fig. 5.12 Effects of Band width on numerical integration (70 hz to 400 hz)

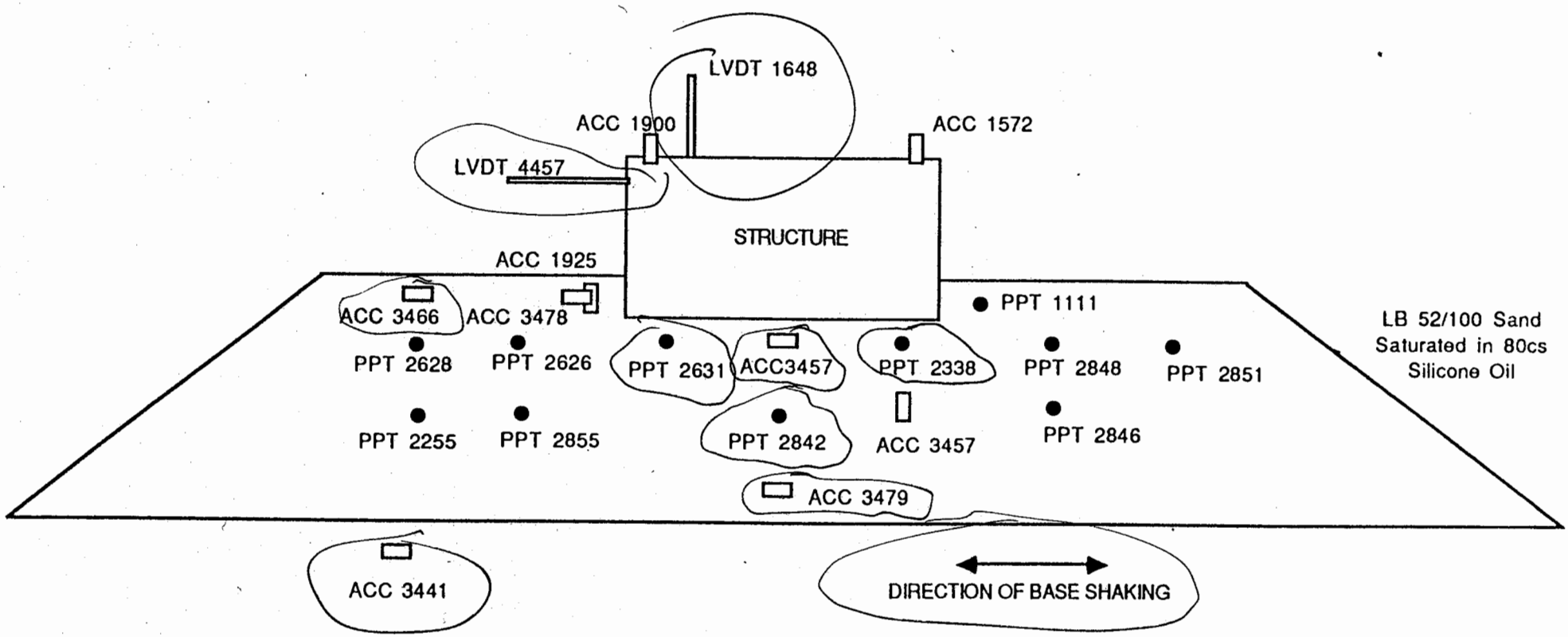

Fig. 6.1 Section of centrifuge model RSS111

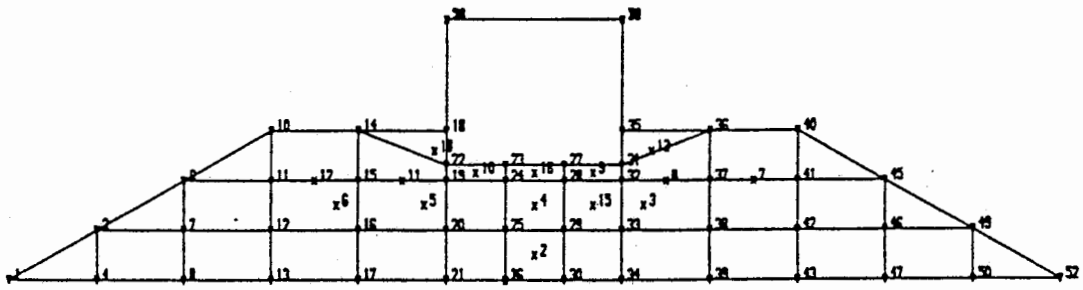

Fig. 6.3 Finite element mesh with plot points

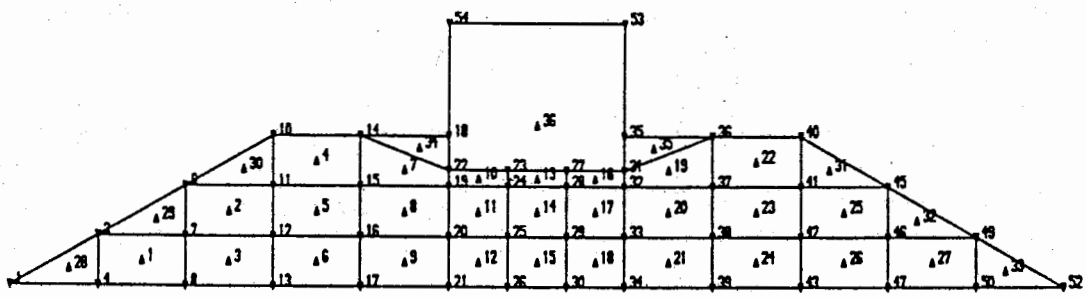

Fig. 6.2 Finite element discretisation

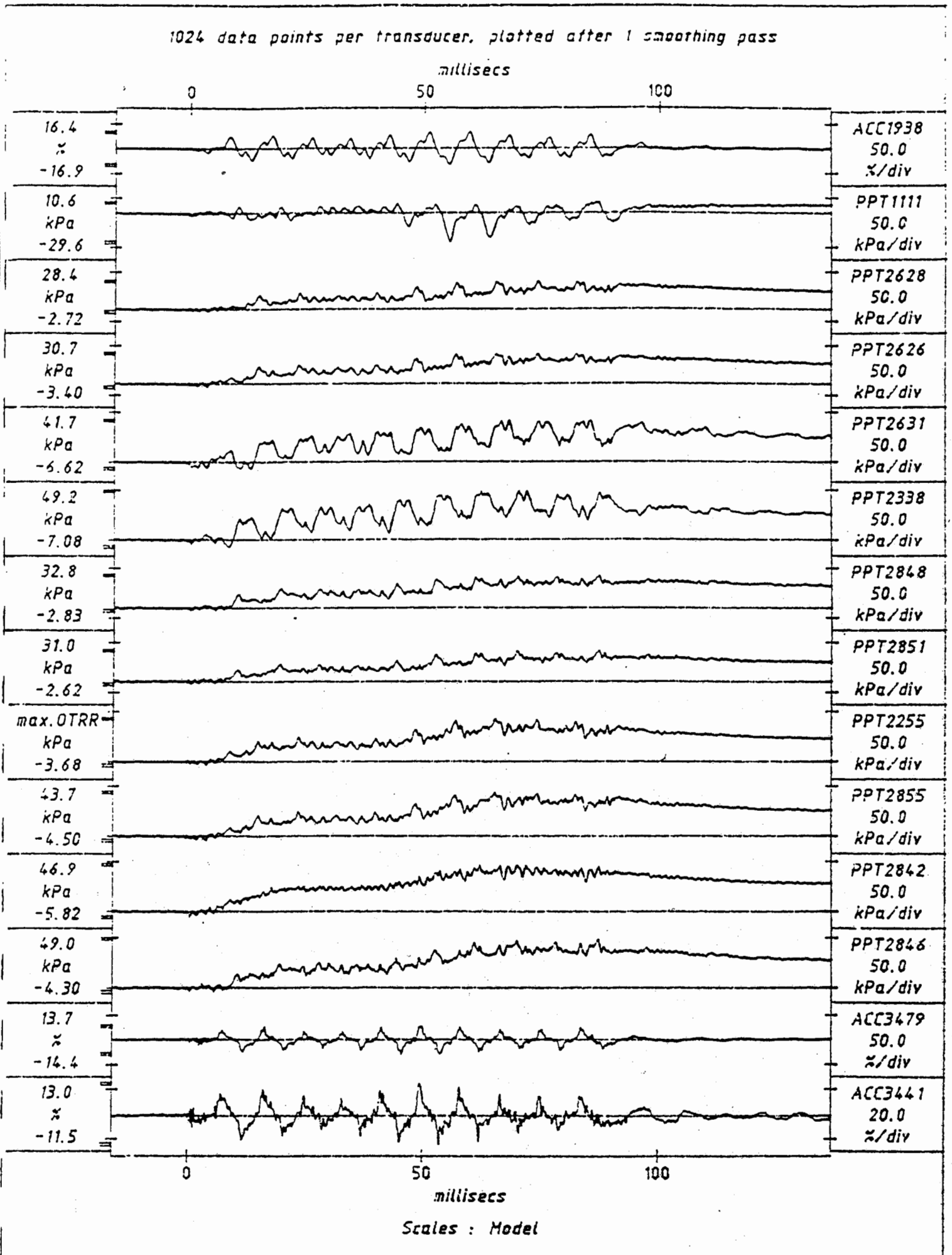

Scales : Model

TEST RSS111 MODEL SAT SURA	EQ1	SHORT-TERM TIME RECORDS	G = 79.0g Km = 12.3%	FIG.NO. 6.4

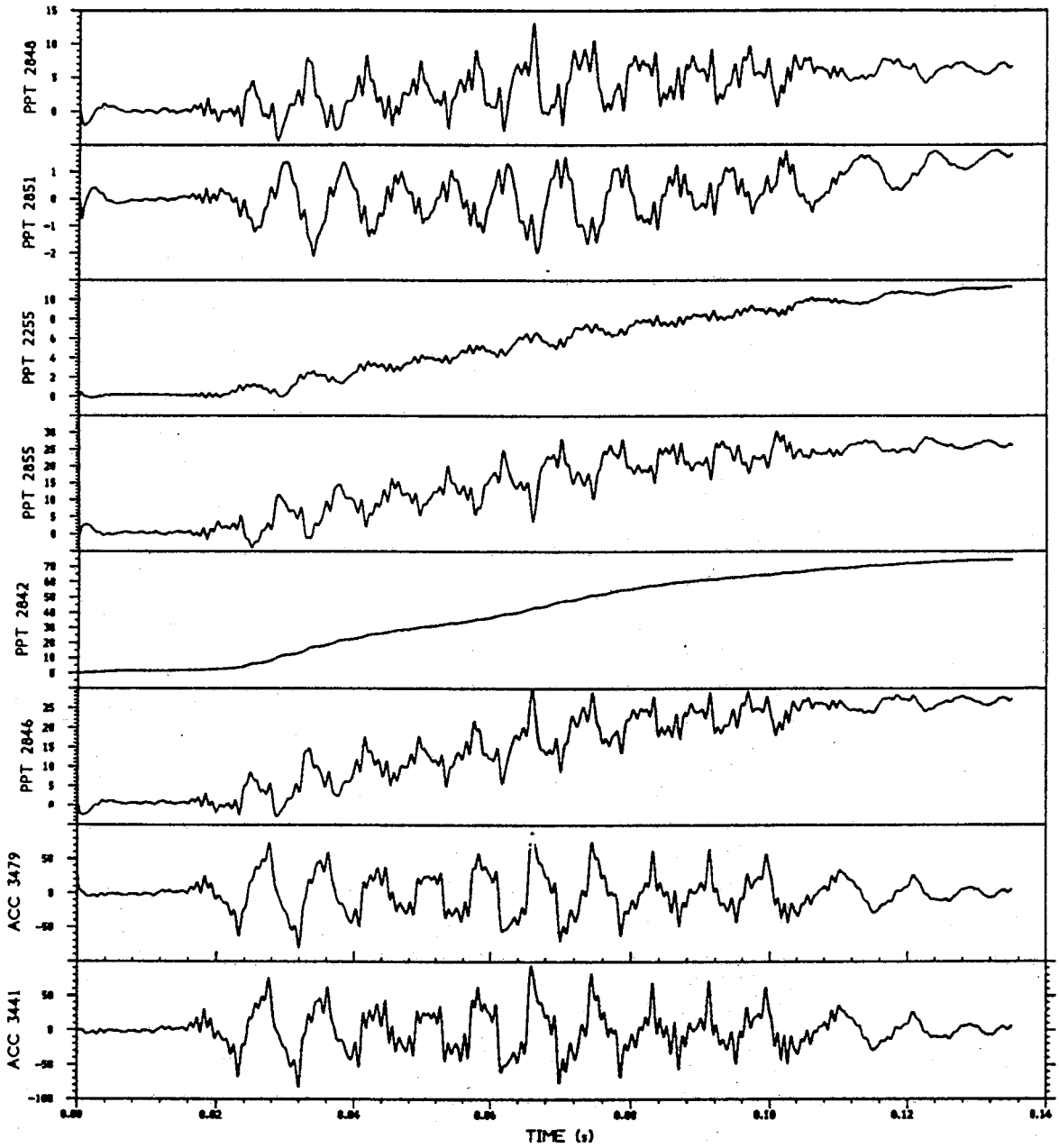

Fig. 6.5 Numerical analysis for Test RSS111 - EQ. NO: 1

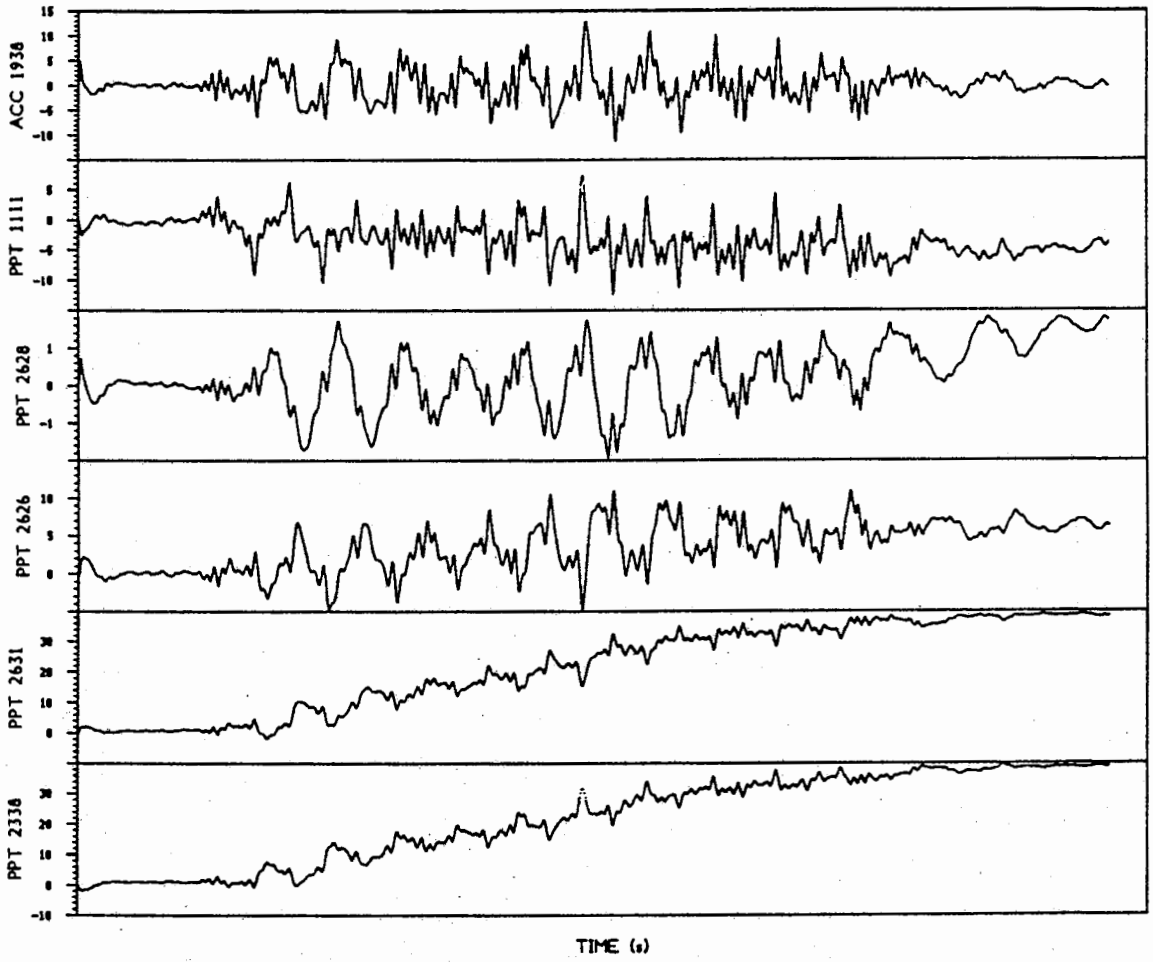

Fig. 6.5 Numerical analysis for Test RSS111 - EQ. NO: 1 (cont.)

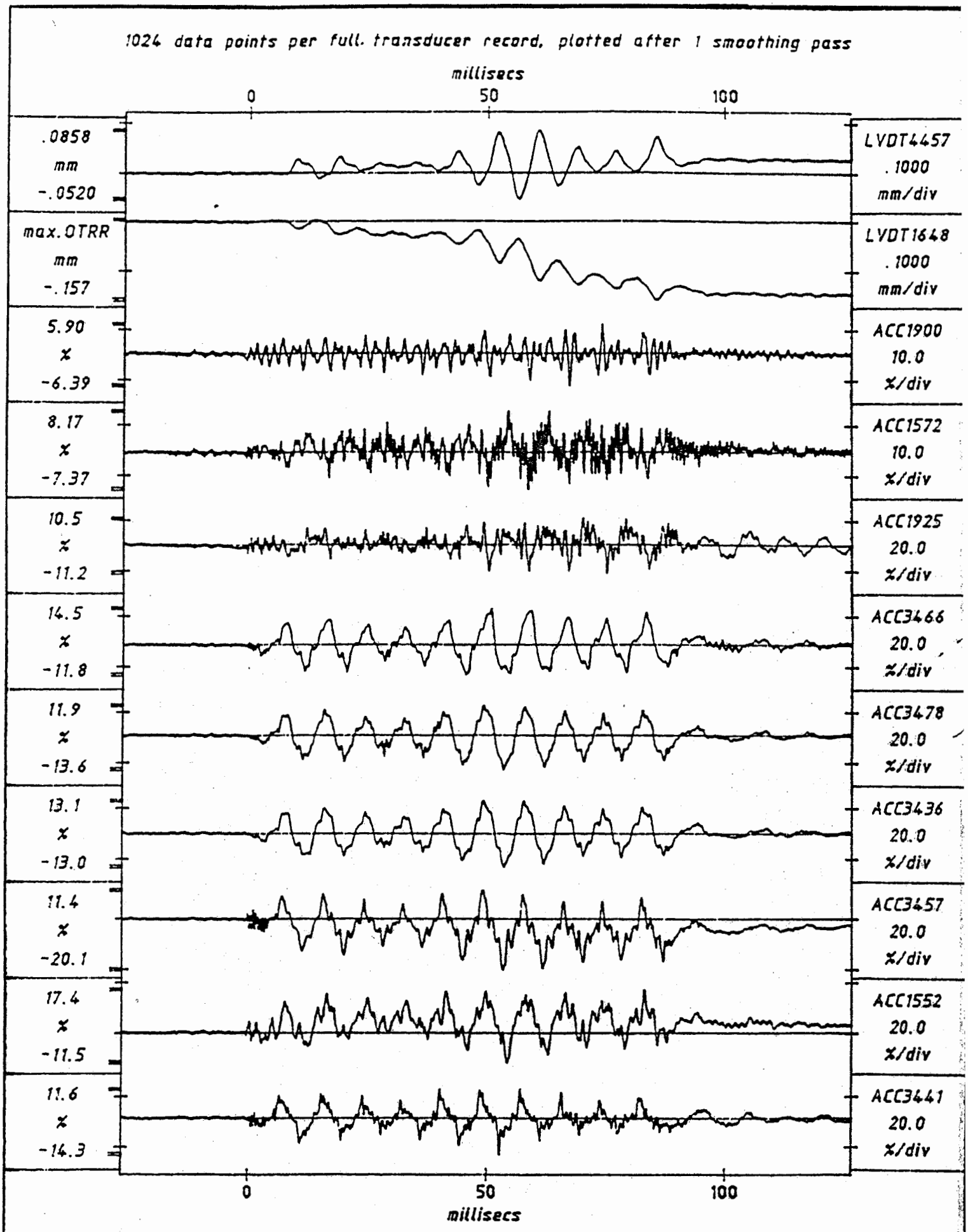

Scales : Model

TEST RSS111 MODEL SAT SURB FLIGHT 1	EQ1	SHORT-TERM TIME RECORDS	G = 79.0g Km = 12.9% Kp = 14.3%	FIG. NO. 6.6

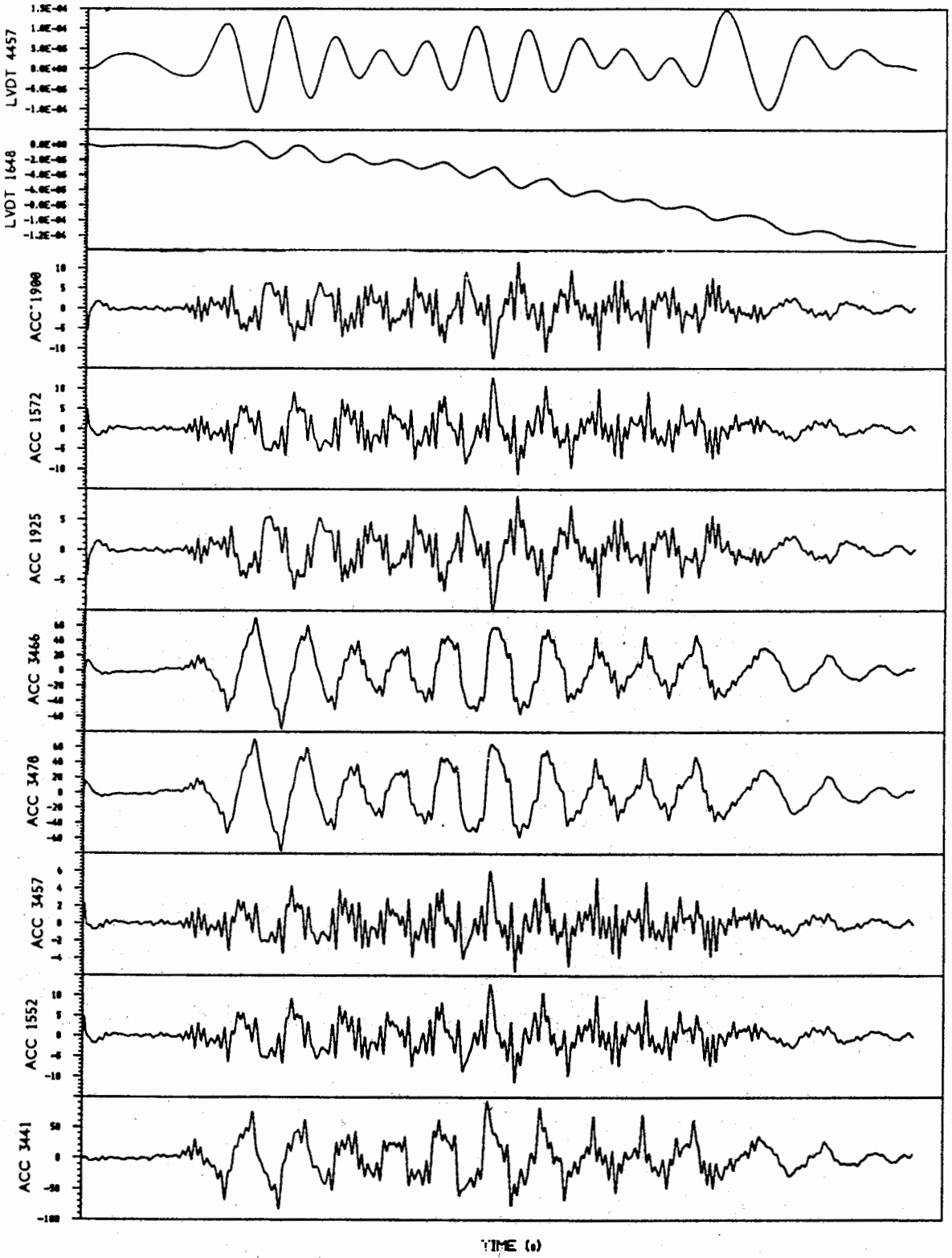

Fig. 6.7 Numerical analysis for Test RSS111 - EQ. NO: 1

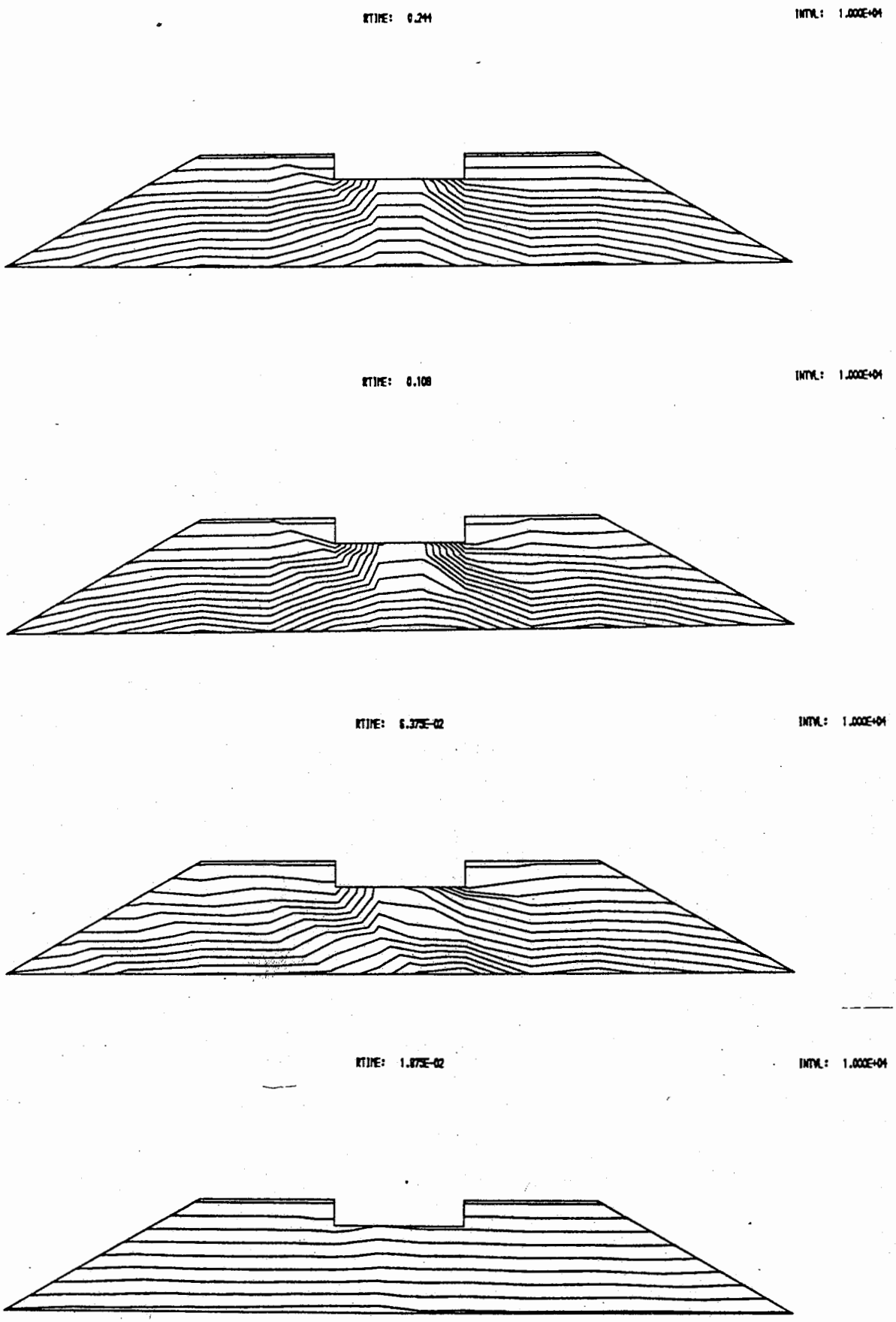

Fig. 6.8 Total pore pressure contours during earthquake 1

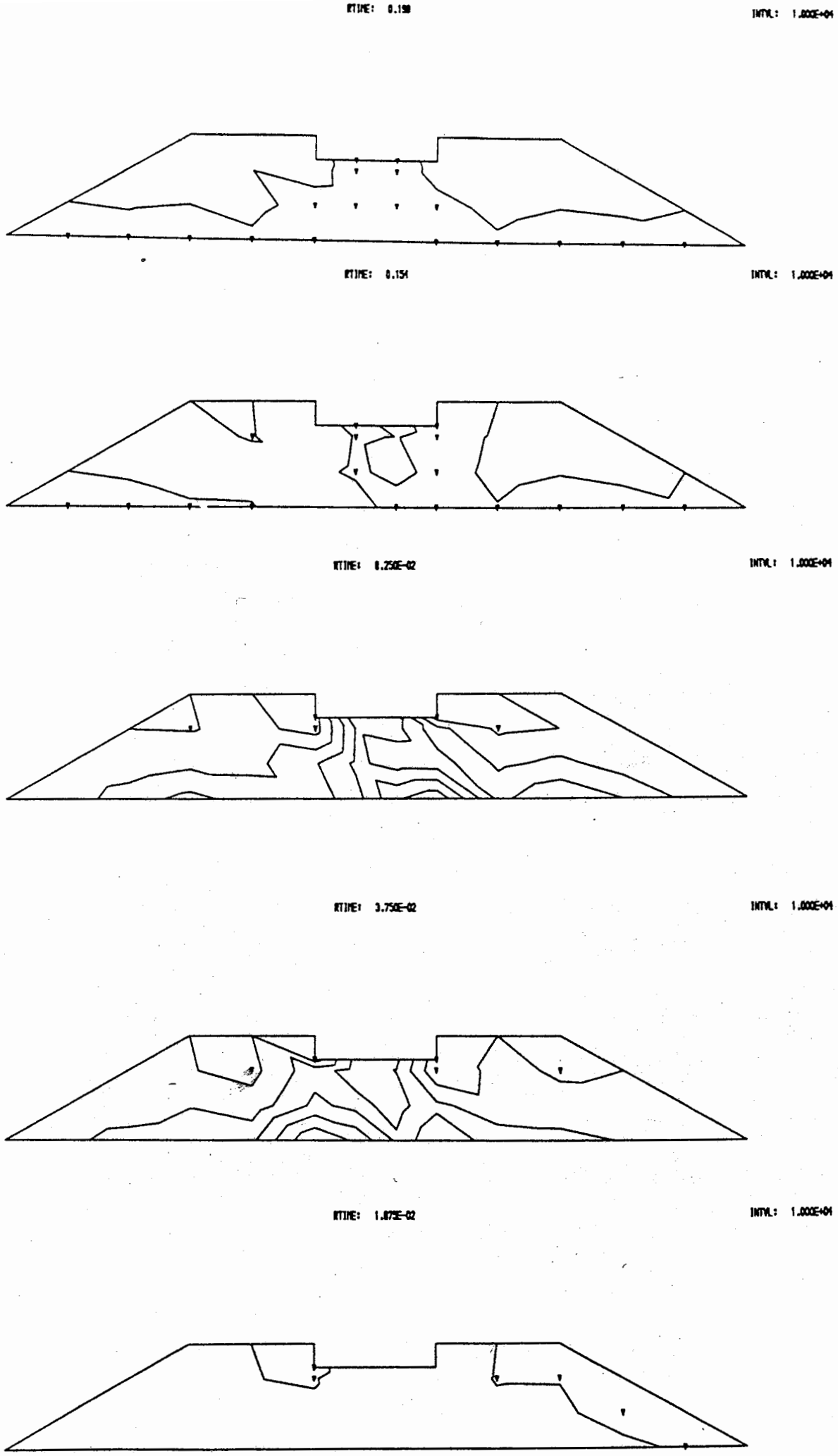

Fig. 6.9 Excess pore pressure contours during earthquake 1

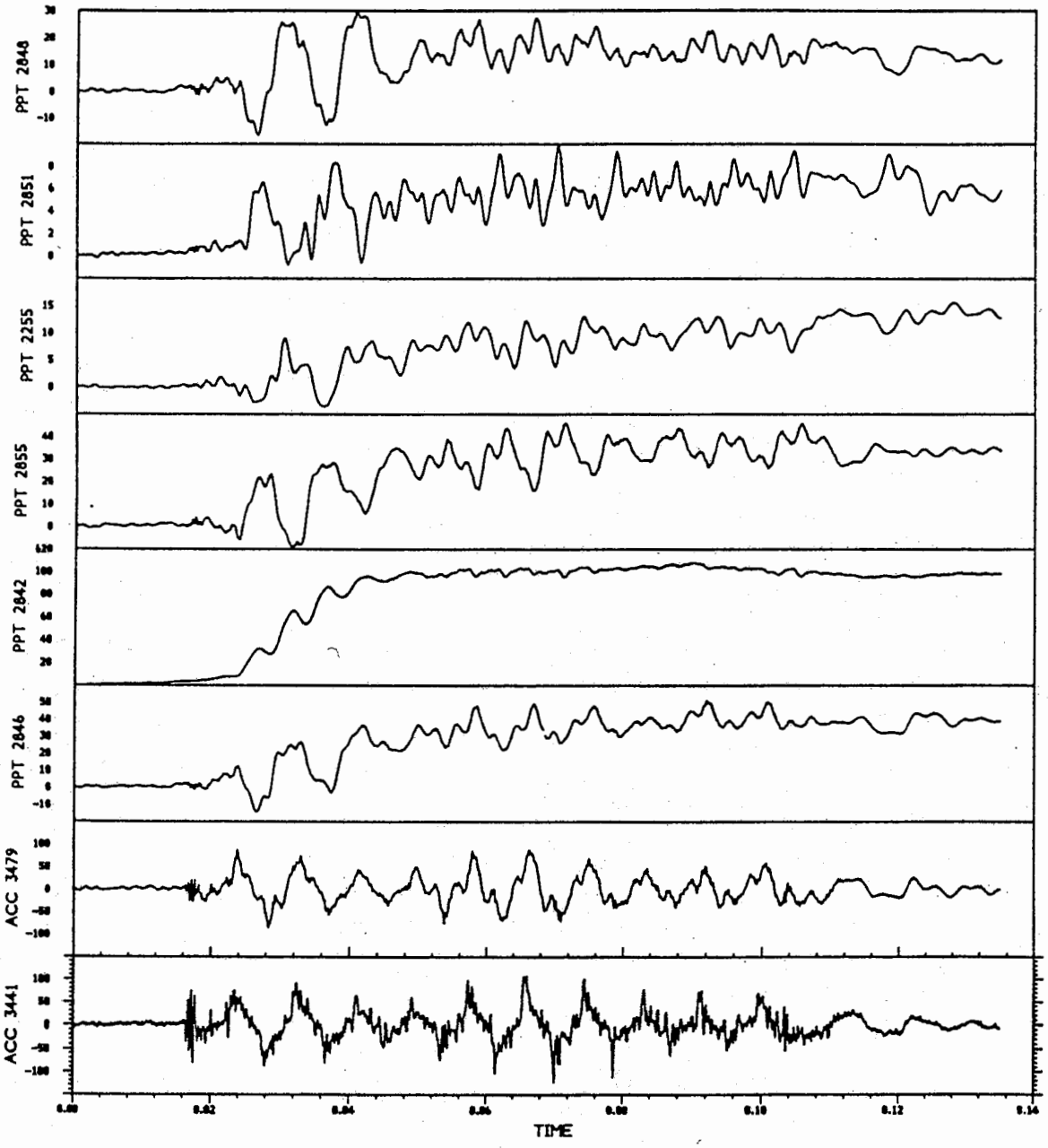

Fig. 6.10 Numerical analysis of Test RSS111- EQ. NO:1 (Zero initial conditions)

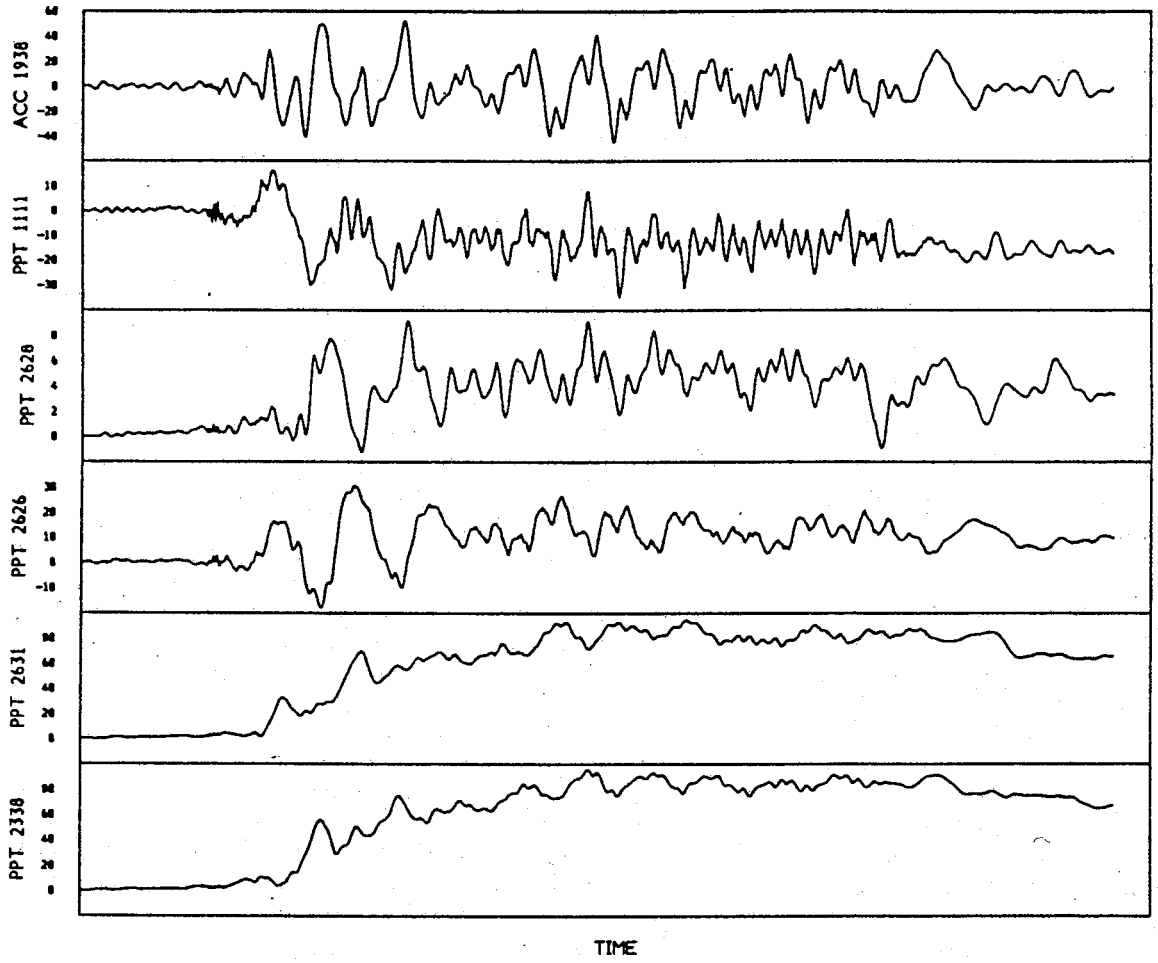

Fig. 6.10 Numerical analysis of Test RSS111- EQ. NO:1 (Zero initial conditions)

(cont.)

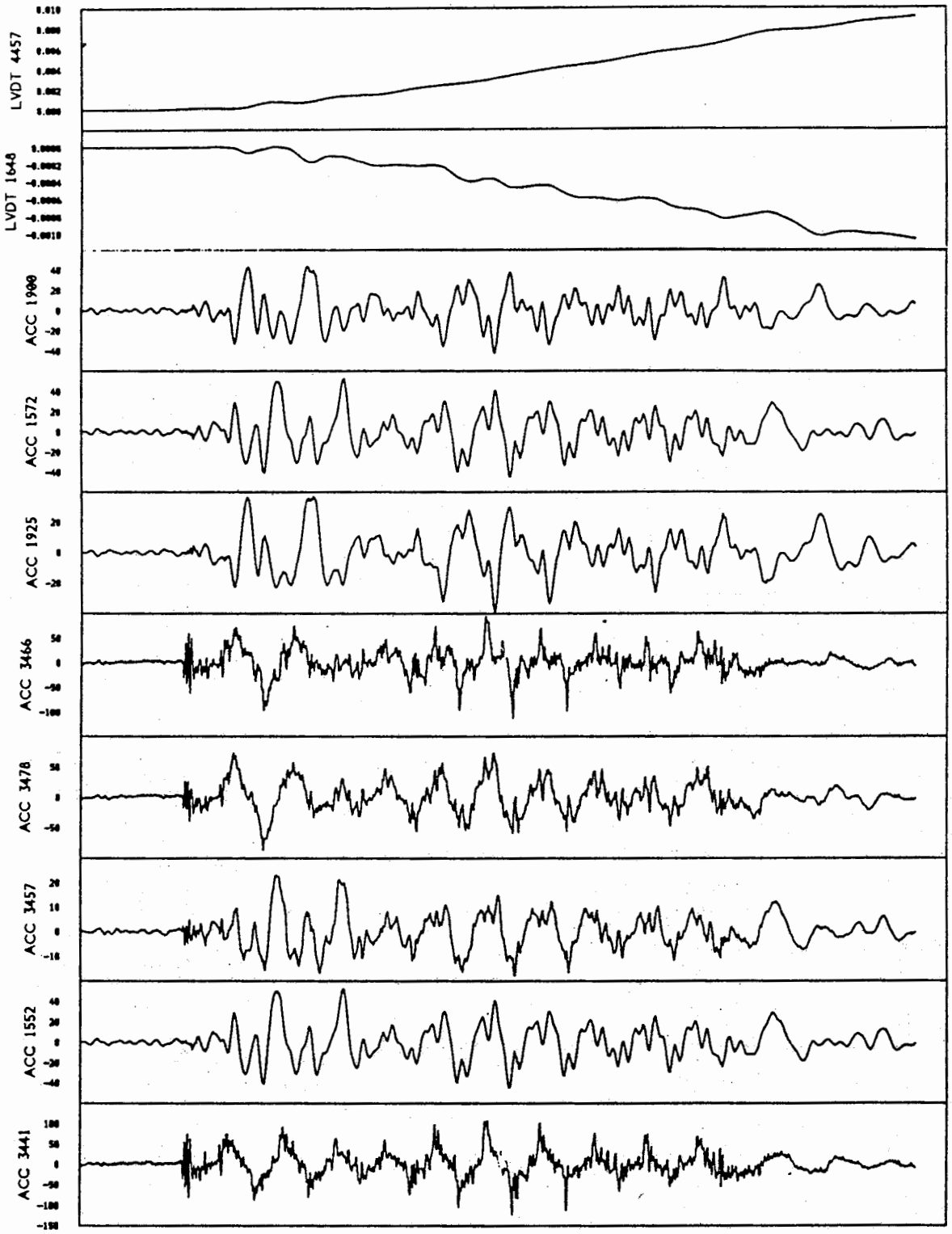

Fig. 6.10 Numerical analysis of Test RSS111- EQ. NO:1 (Zero initial conditions)

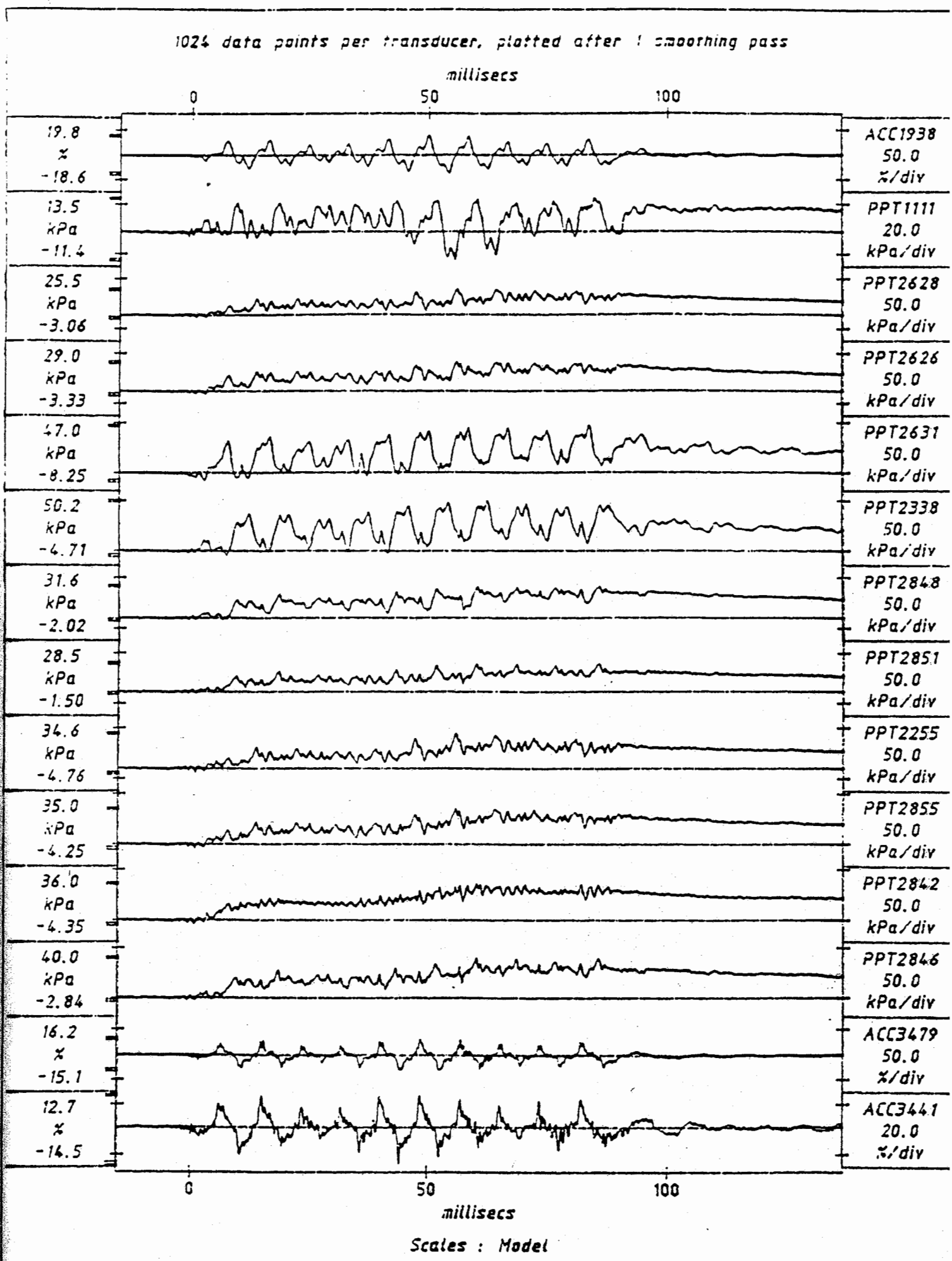

TEST RSS111 MODEL SAT SURA	EQ2	SHORT-TERM TIME RECORDS	G = 79.0g Km = 13.6%	FIG. NO.

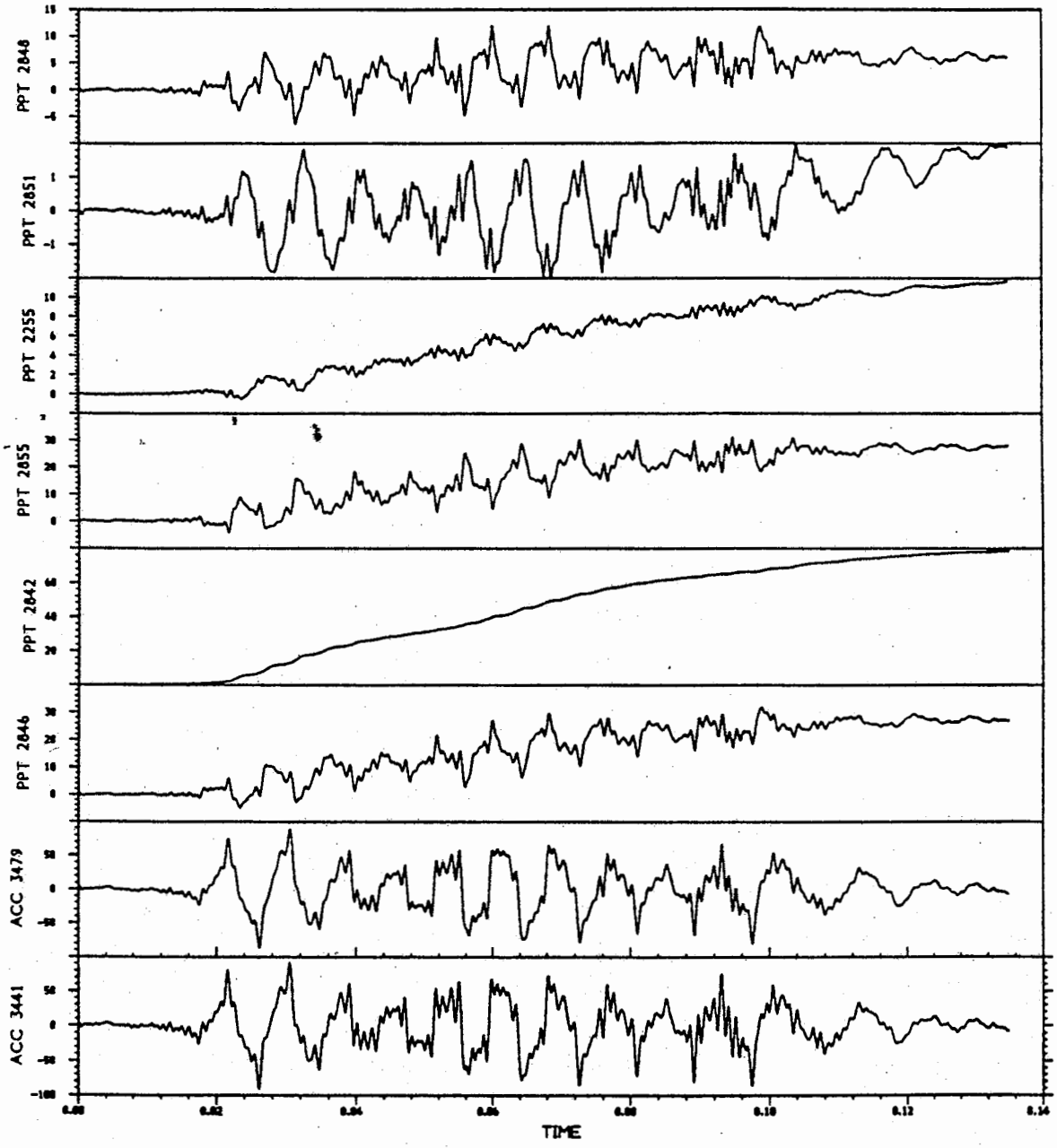

Fig. 6.12 Numerical analysis for Test RSS111 - EQ. NO: 2

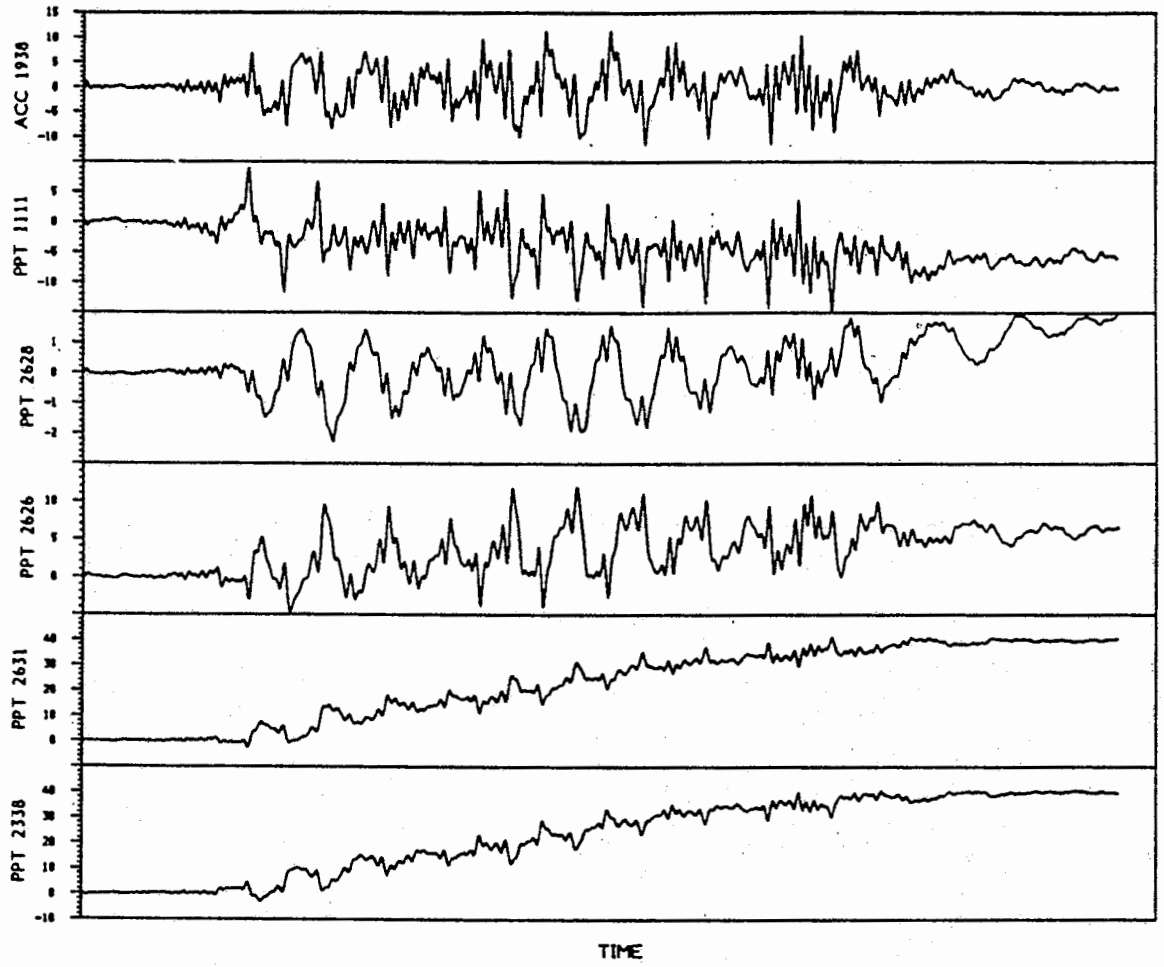

Fig. 6.12 Numerical analysis for Test RSS111 - EQ. NO: 2 (cont.)

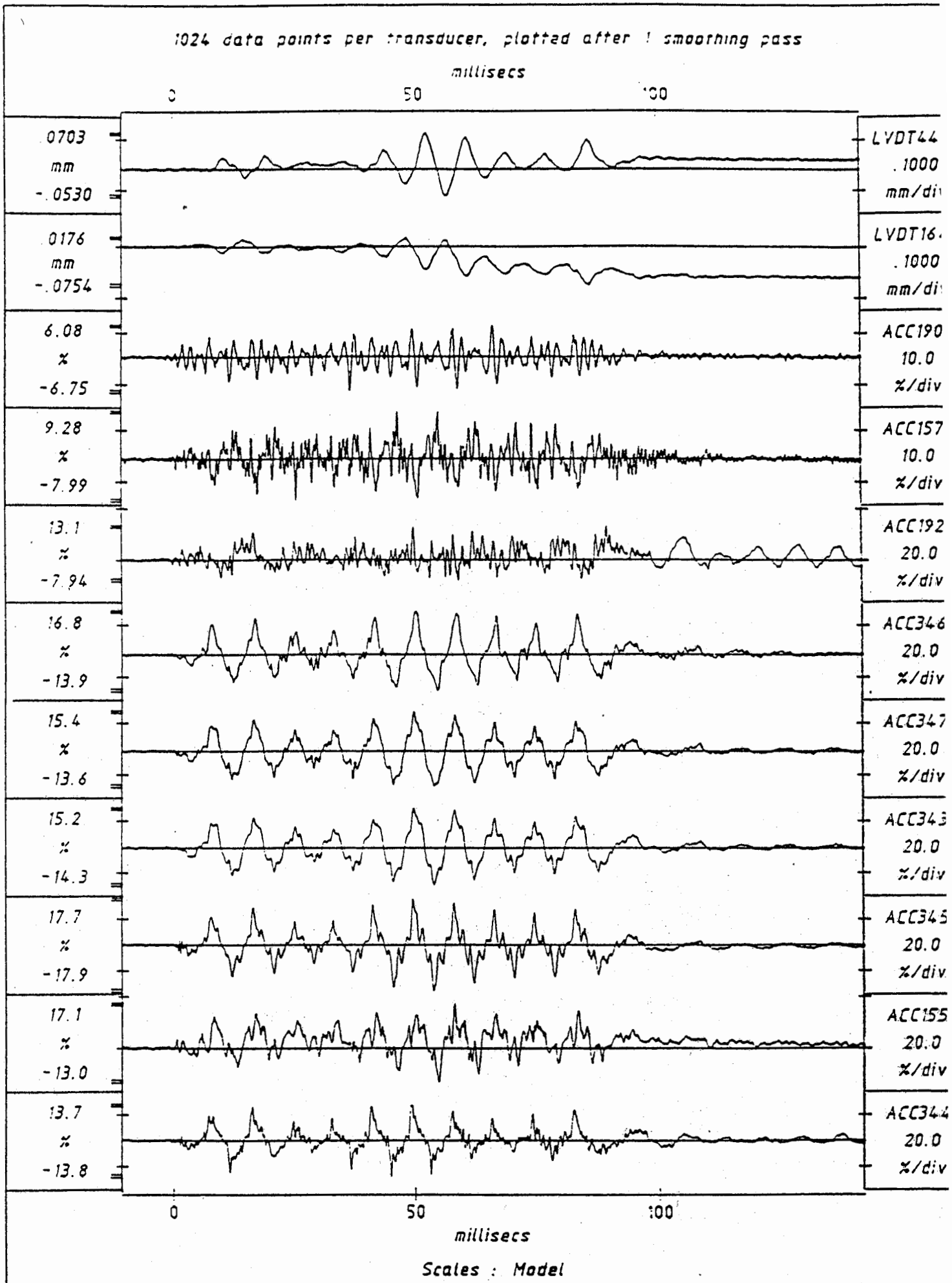

Scales : Model

TEST RSS111 MODEL SAT SURB FLIGHT 1	EQ2	SHORT-TERM TIME RECORDS	G = 79.0g Km = 13.8% Kp = 13.8%	FIG. A 6.13

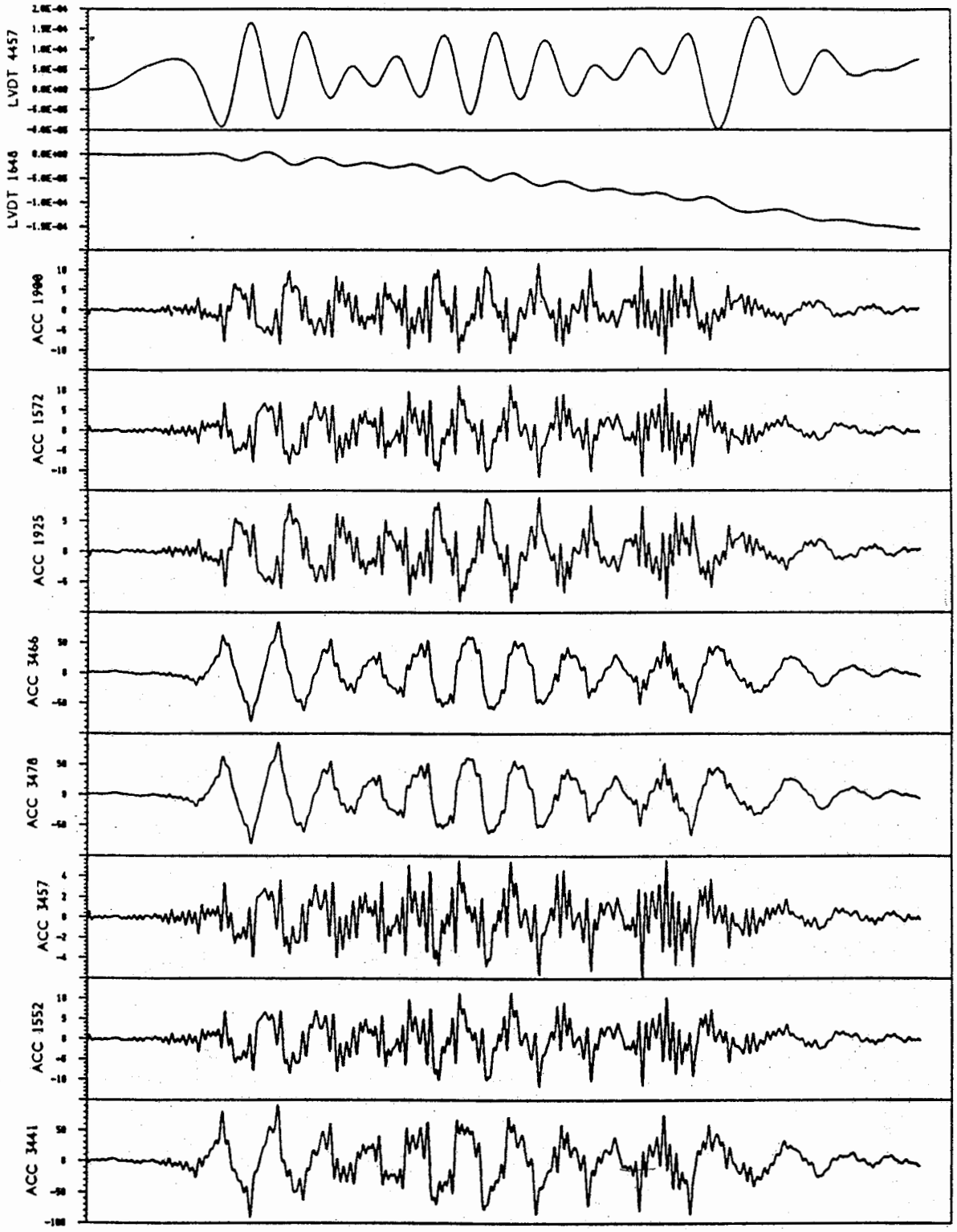

Fig. 6.14 Numerical analysis for Test RSS111 - EQ. NO: 2

1024 data points per transducer, plotted after 1 smoothing pass

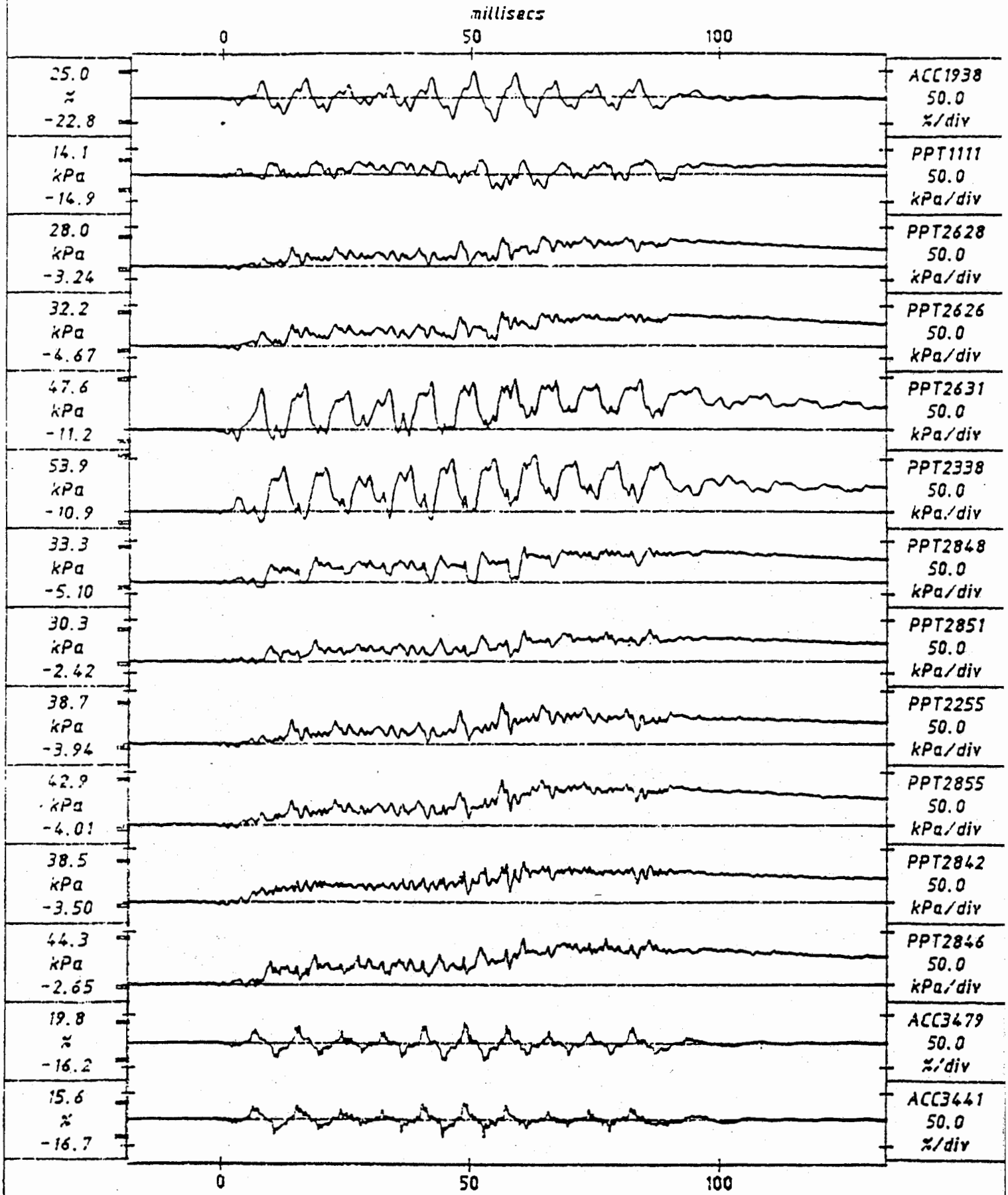

Scales : Model

TEST RSS111 MODEL SAT SURA EQ3	SHORT-TERM	G = 79.0g Km = 16.1%	FIG. NO. 6.15

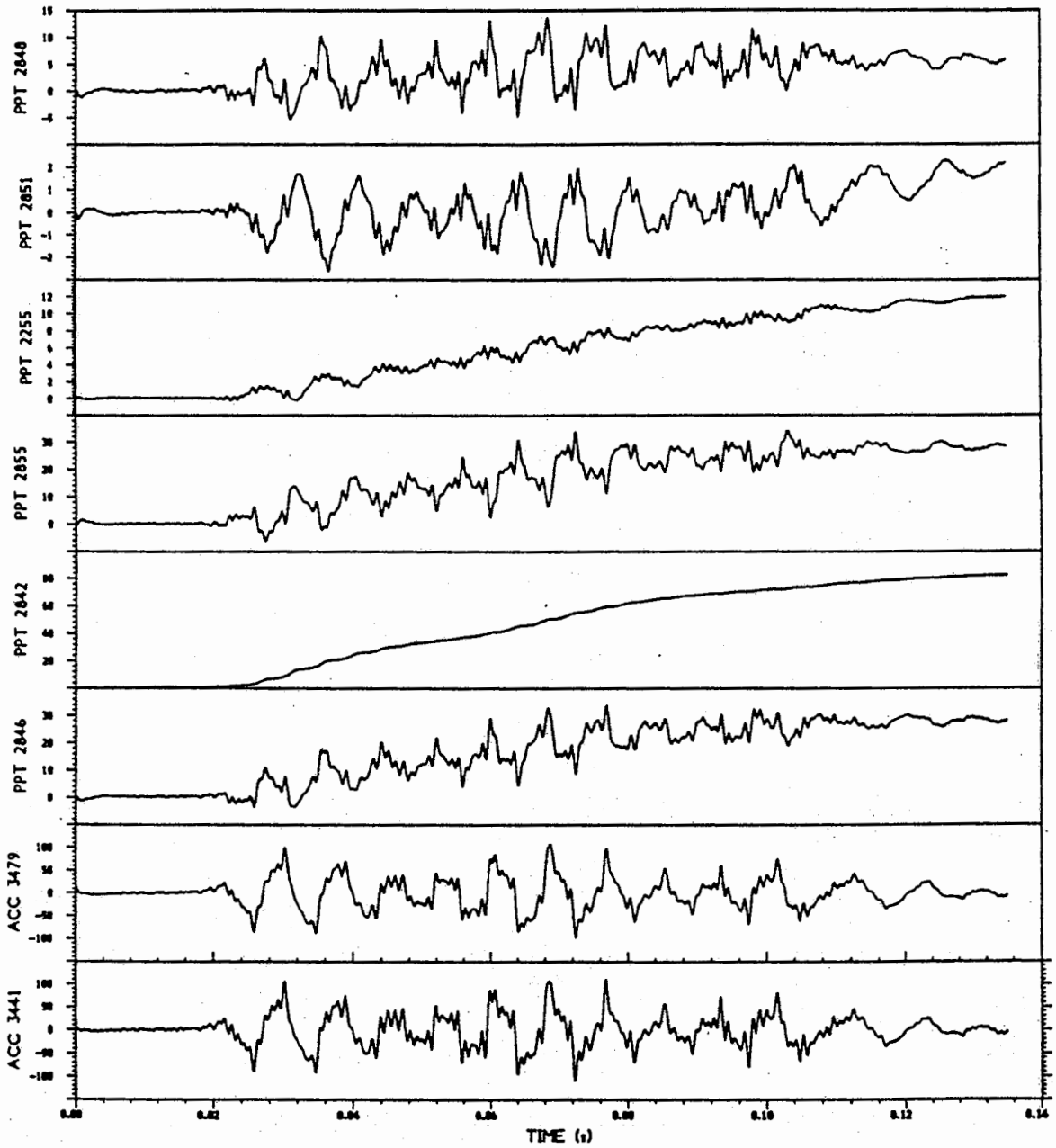

Fig. 6.16 Numerical analysis for Test RSS111 - EQ. NO: 3

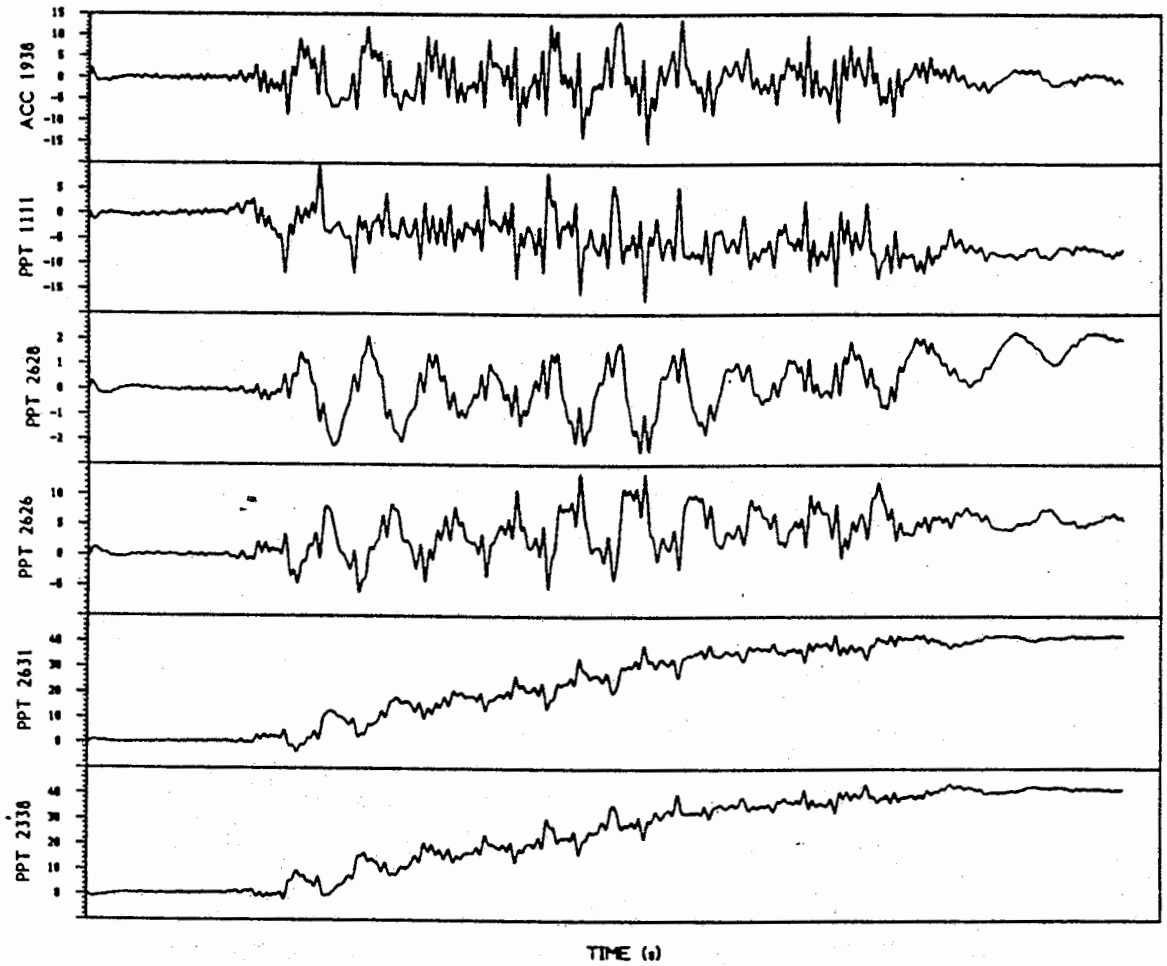

Fig. 6.16 Numerical analysis for Test RSS111 - EQ. NO: 3 (cont.)

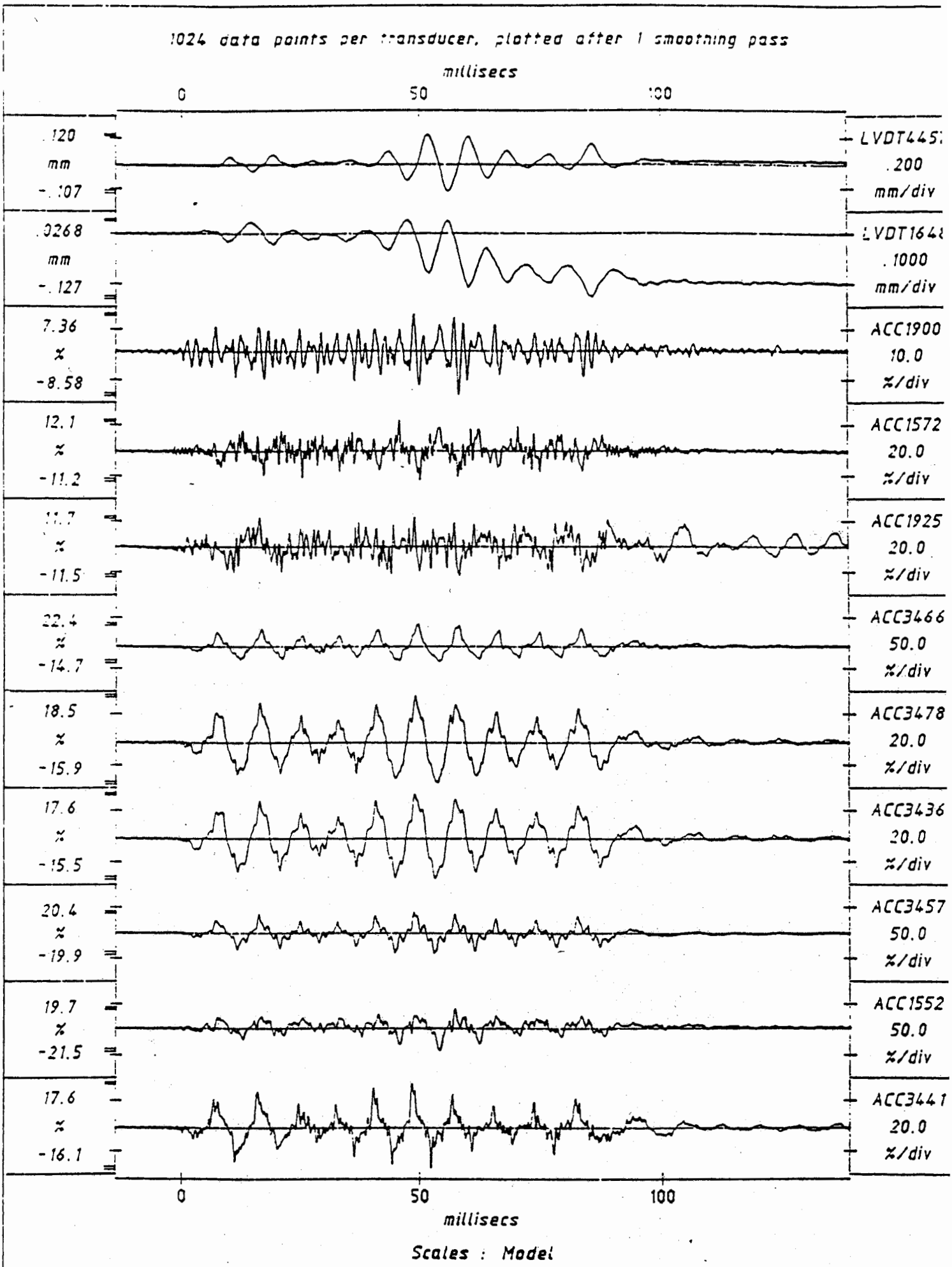

Scales : Model

TEST RSS111 MODEL SAT SURB FLIGHT 1	EQ3	SHORT-TERM TIME RECORDS	G = 79.0g Km = 16.8% Ko = 17.6%	FIG.NO 6.17

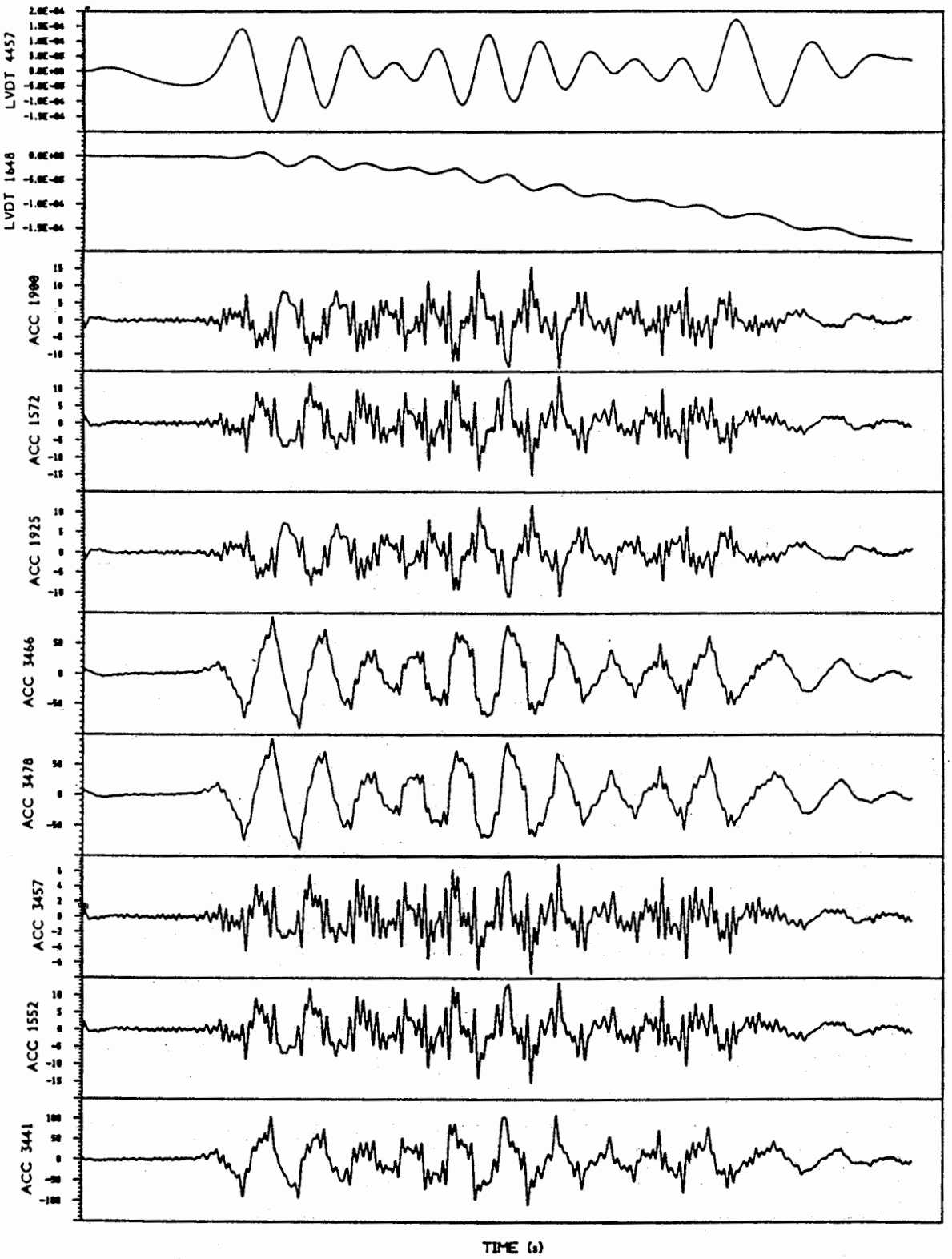

Fig. 6.18 Numerical analysis for Test RSS111 - EQ. NO: 3

1024 data points per transducer, plotted after 1 smoothing pass

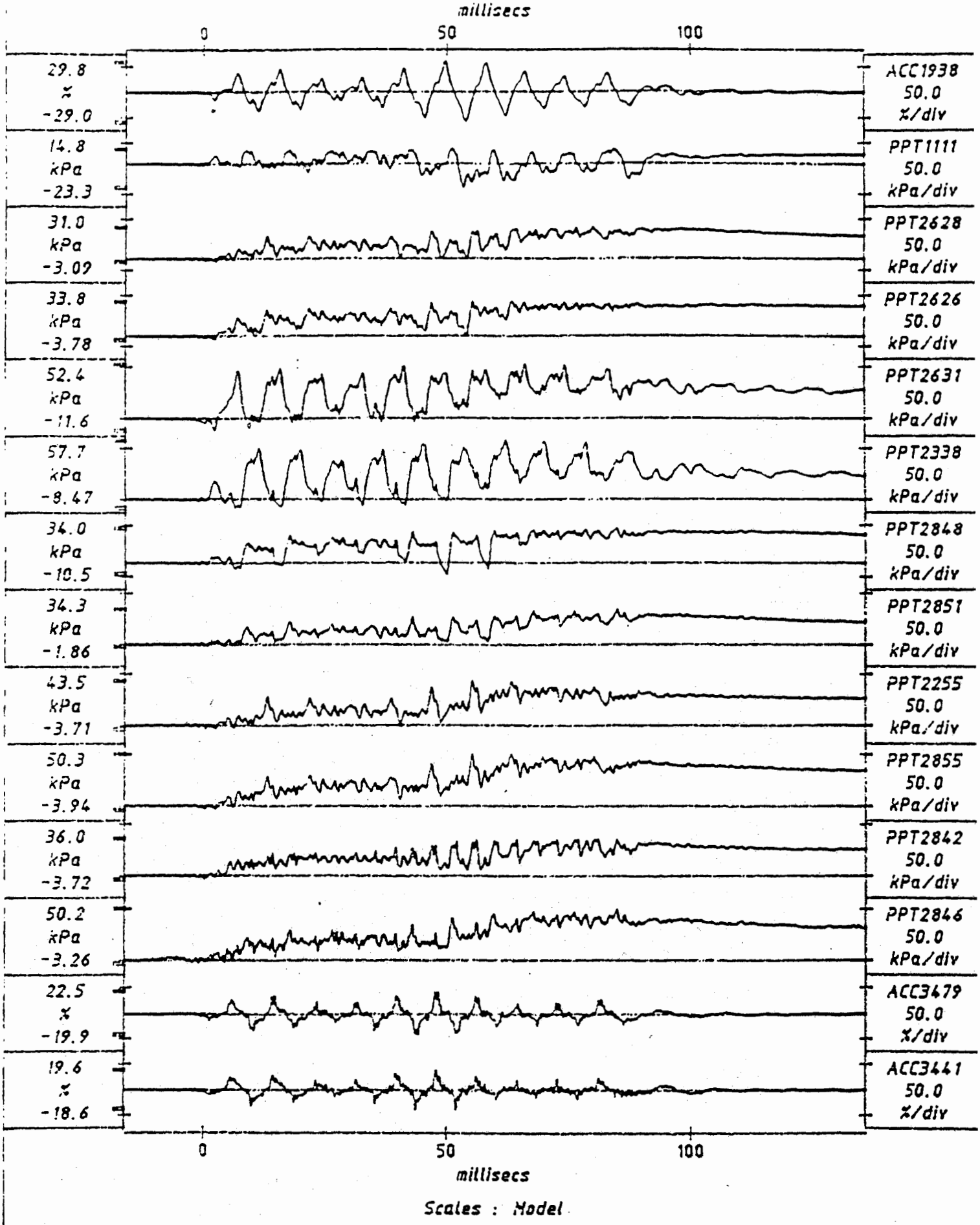

Scales : Model

TEST RSS111 MODEL SAT SURA EQ4	SHORT-TERM	G = 79.0g Km = 19 1%	FIG. NO. 6.19

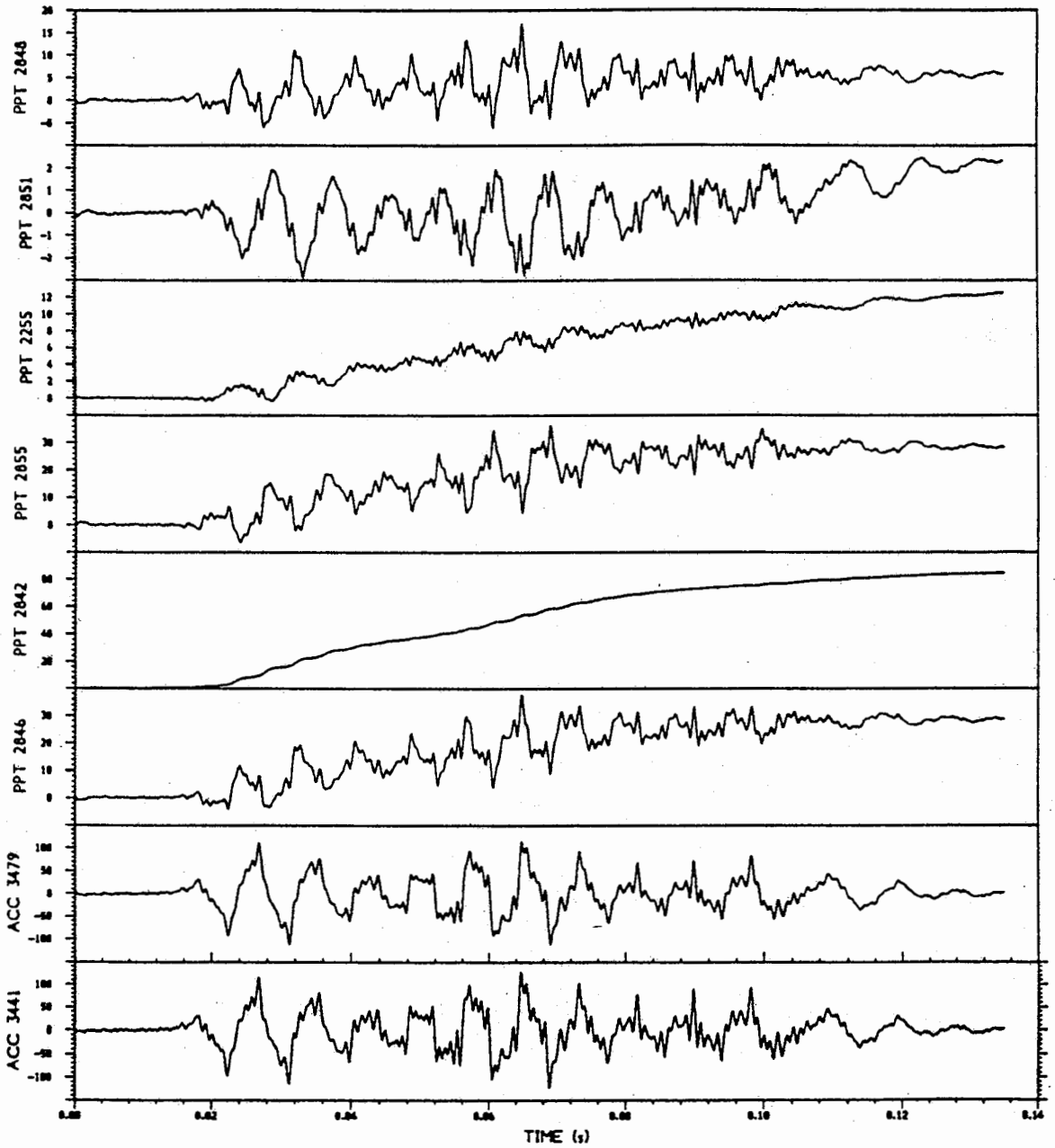

Fig. 6.20 Numerical analysis for Test RSS111 - EQ. NO: 4

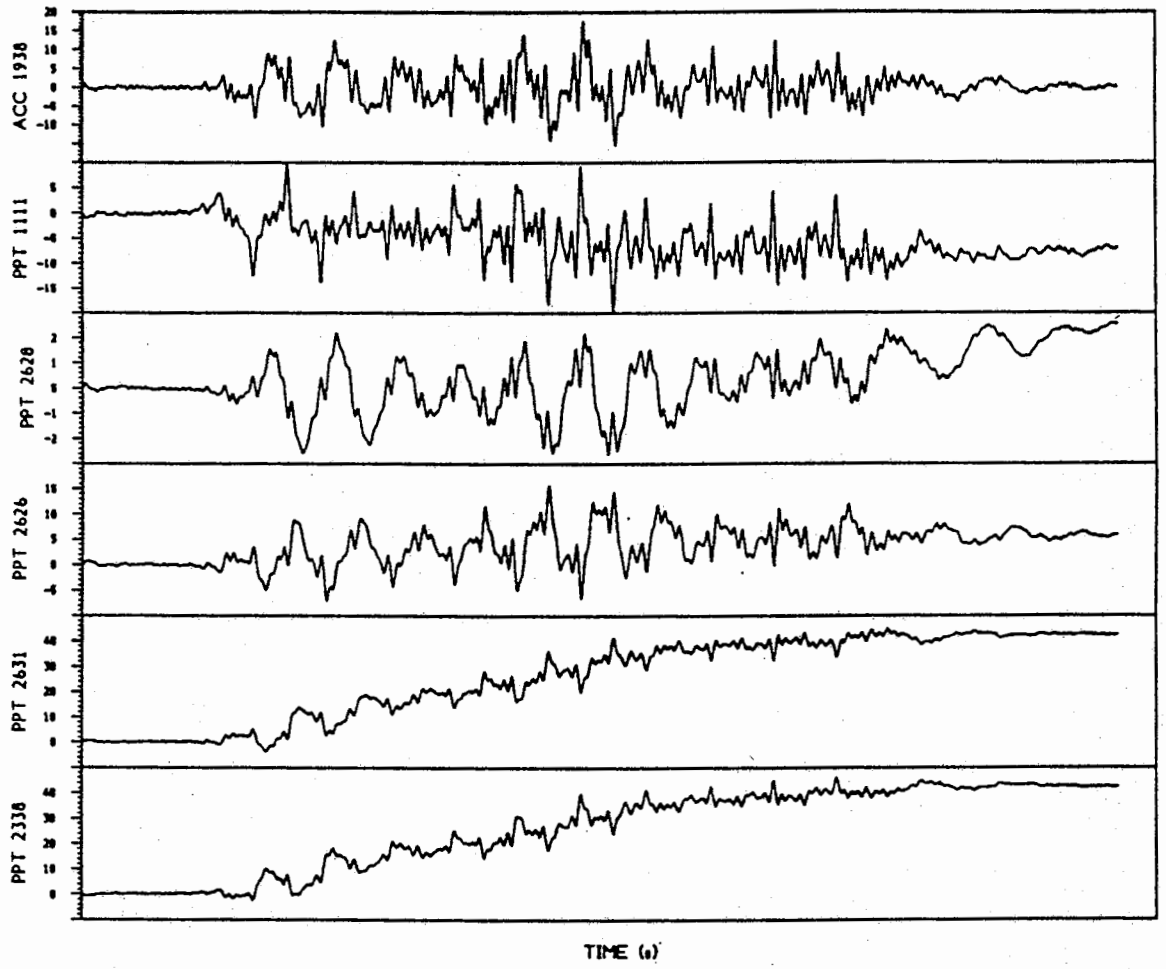

Fig. 6.20 Numerical analysis for Test RSS111 - EQ. NO: 4 (cont.)

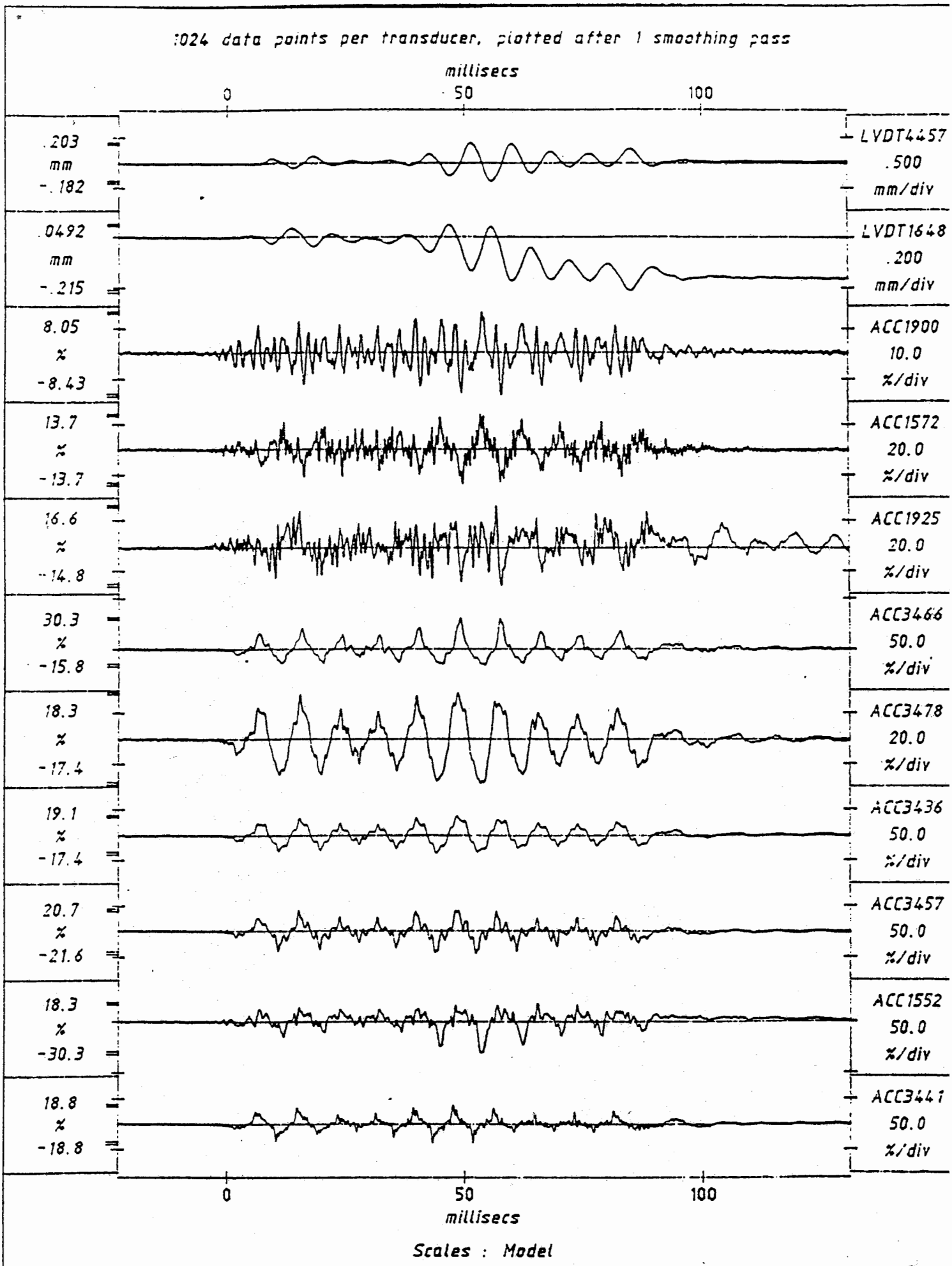

TEST RSS111 MODEL SAT SURB FLIGHT 1	EQ4	SHORT-TERM TIME RECORDS	G = 79.0g Km = 18.8% Kp = 18.8%	FIG.NO 6.21

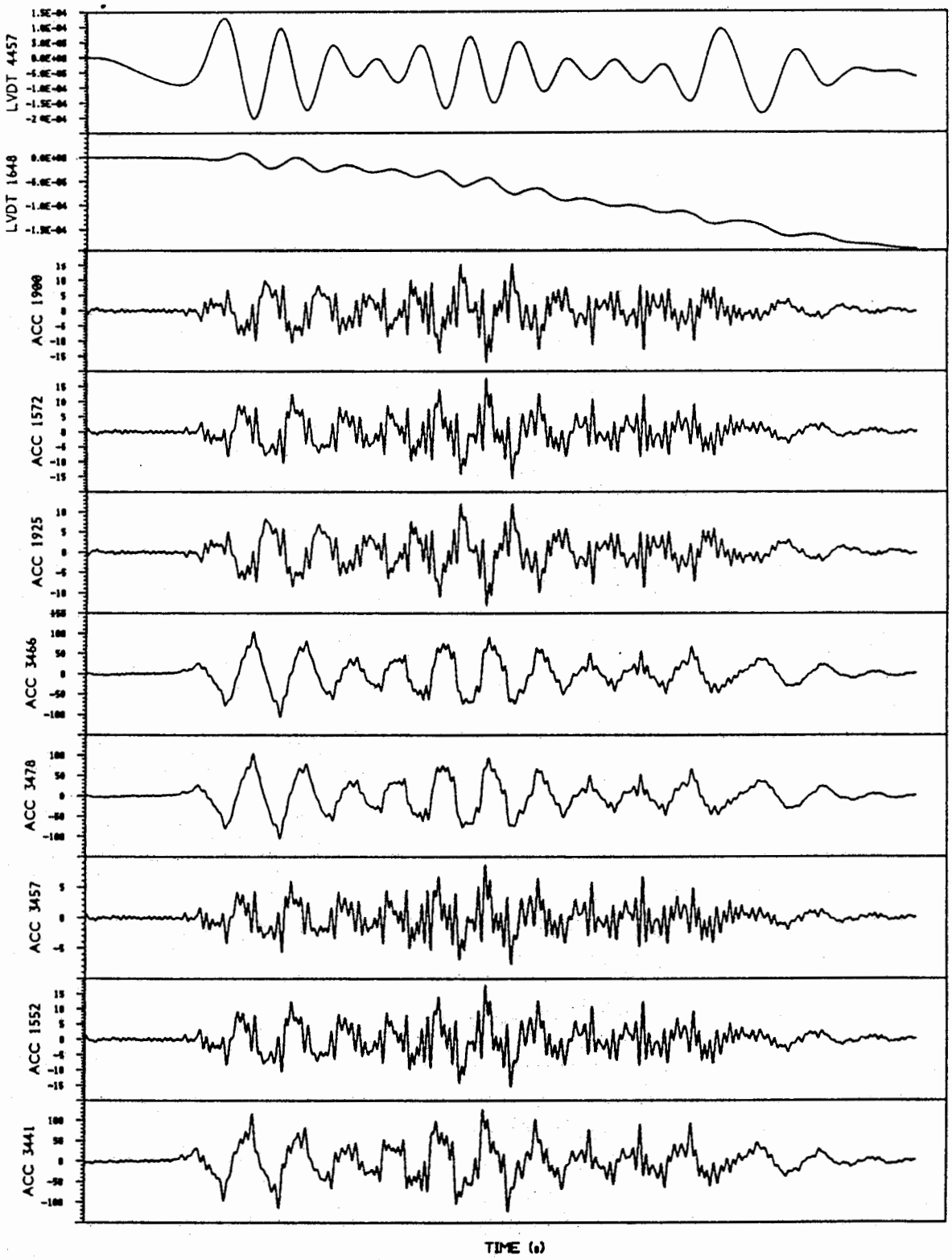

Fig. 6.22 Numerical analysis for Test RSS111 - EQ. NO: 4

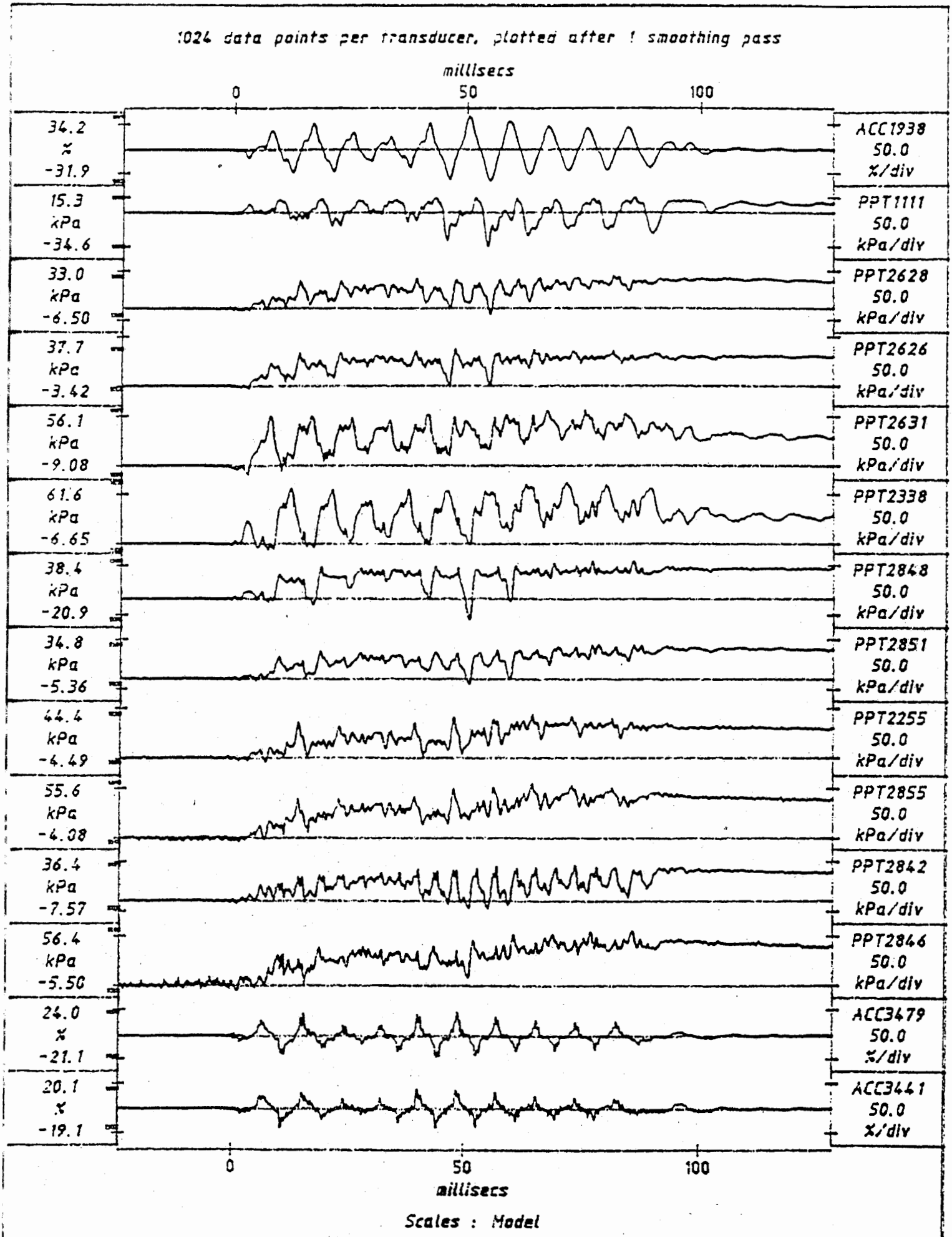

TEST RSS111
MODEL SAT SURA EQ5

SHORT-TERM

G = 79.0g
Km = 19.6%

FIG.NO.

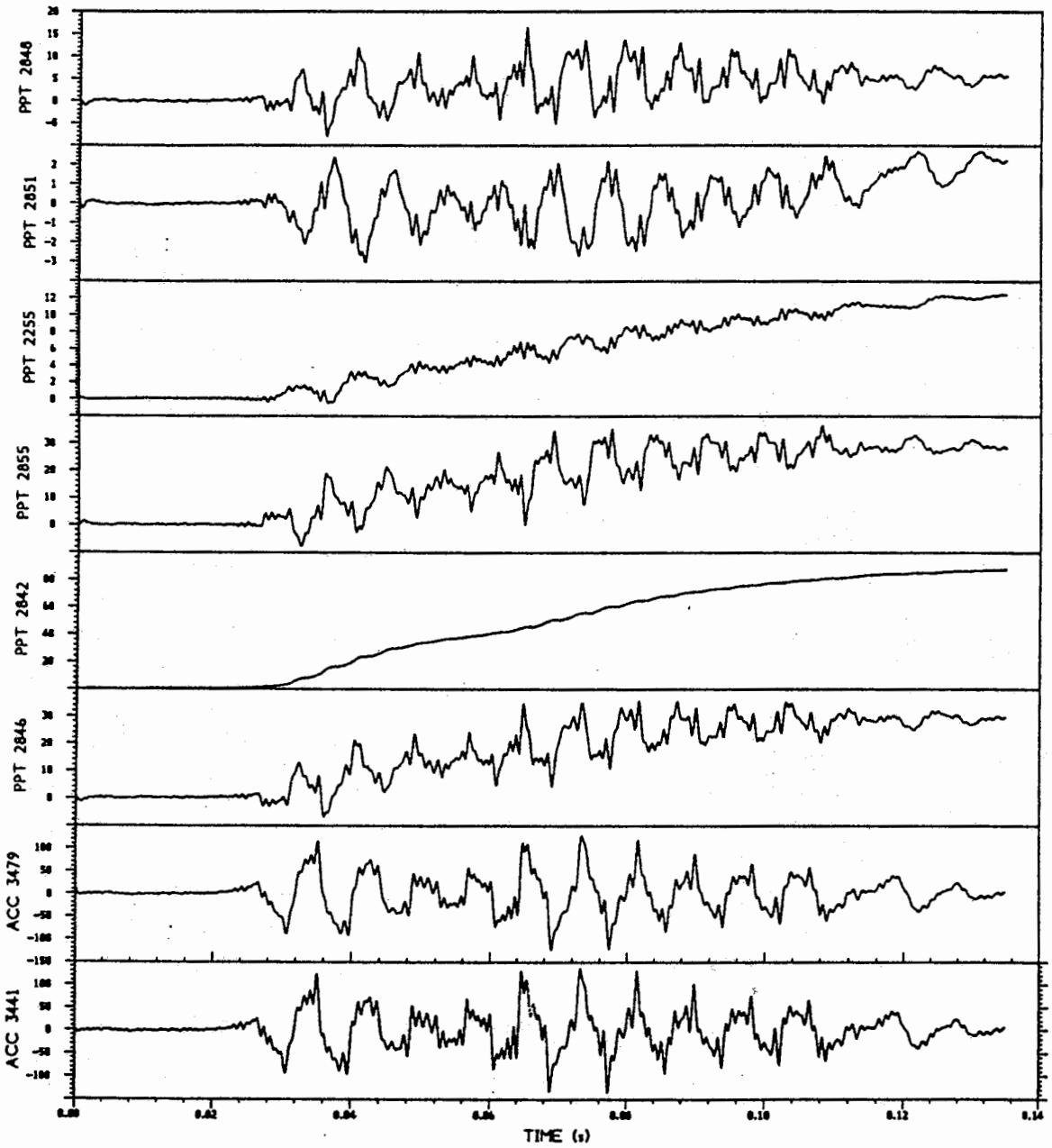

Fig. 6.24 Numerical analysis for Test RSS111 - EQ. NO: 5

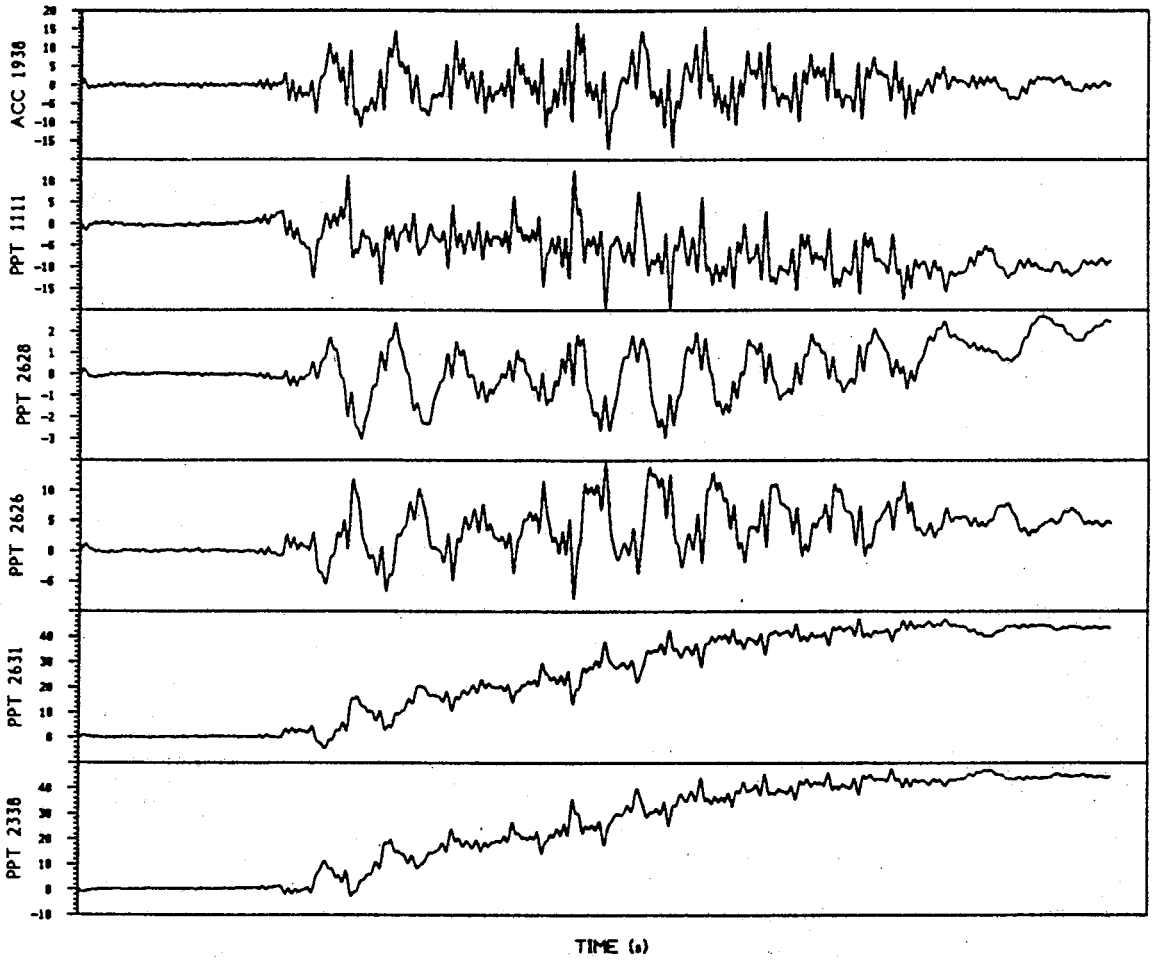

Fig. 6.24 Numerical analysis for Test RSS111 - EQ. NO: 5 (cont.)

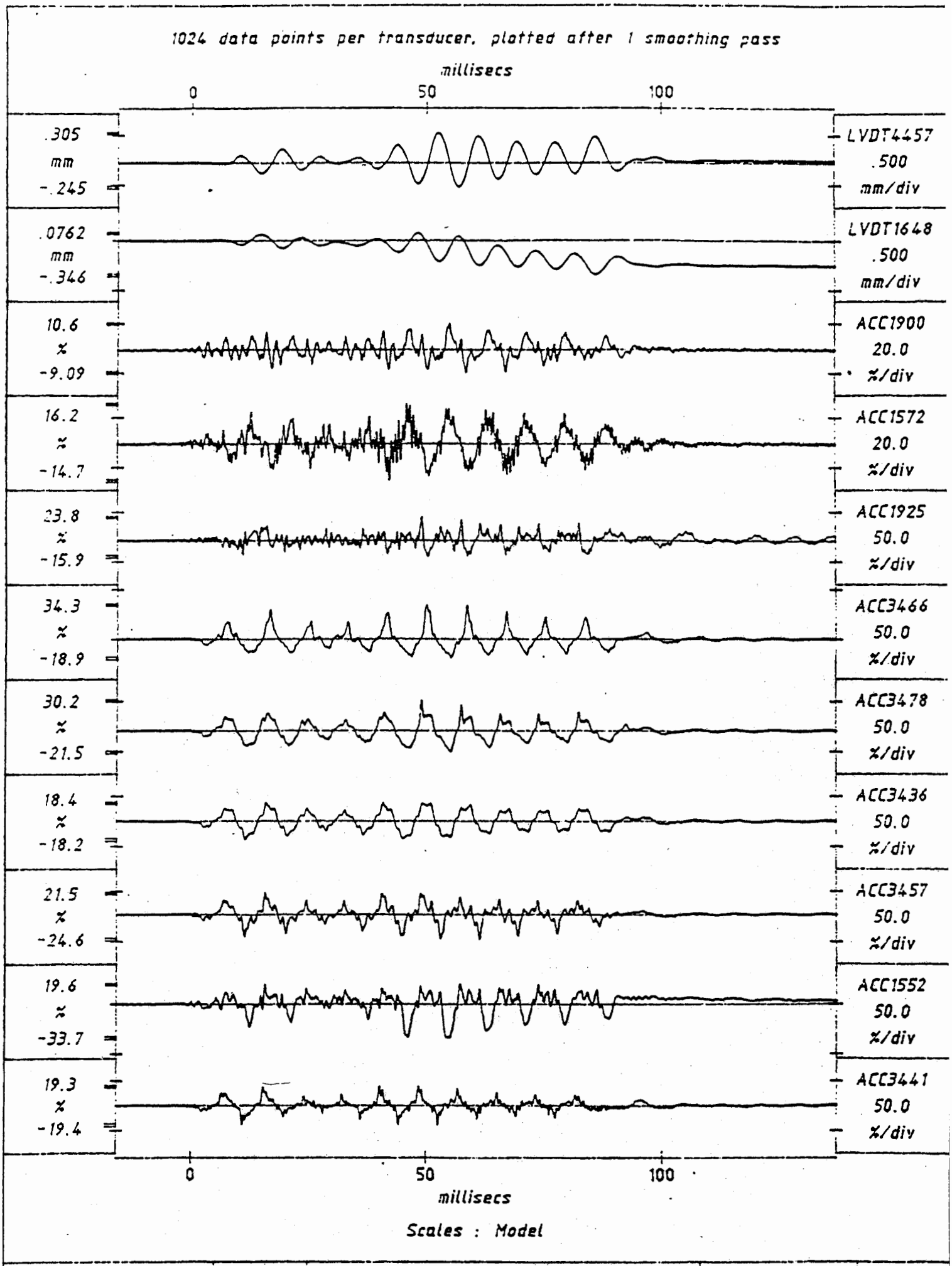

TEST RSS111 MODEL SAT SURB FLIGHT 1	EQ5	SHORT-TERM TIME RECORDS	G = 79.0g Km = 19.4% Kp = 19.4%	FIG. NO. 6.25

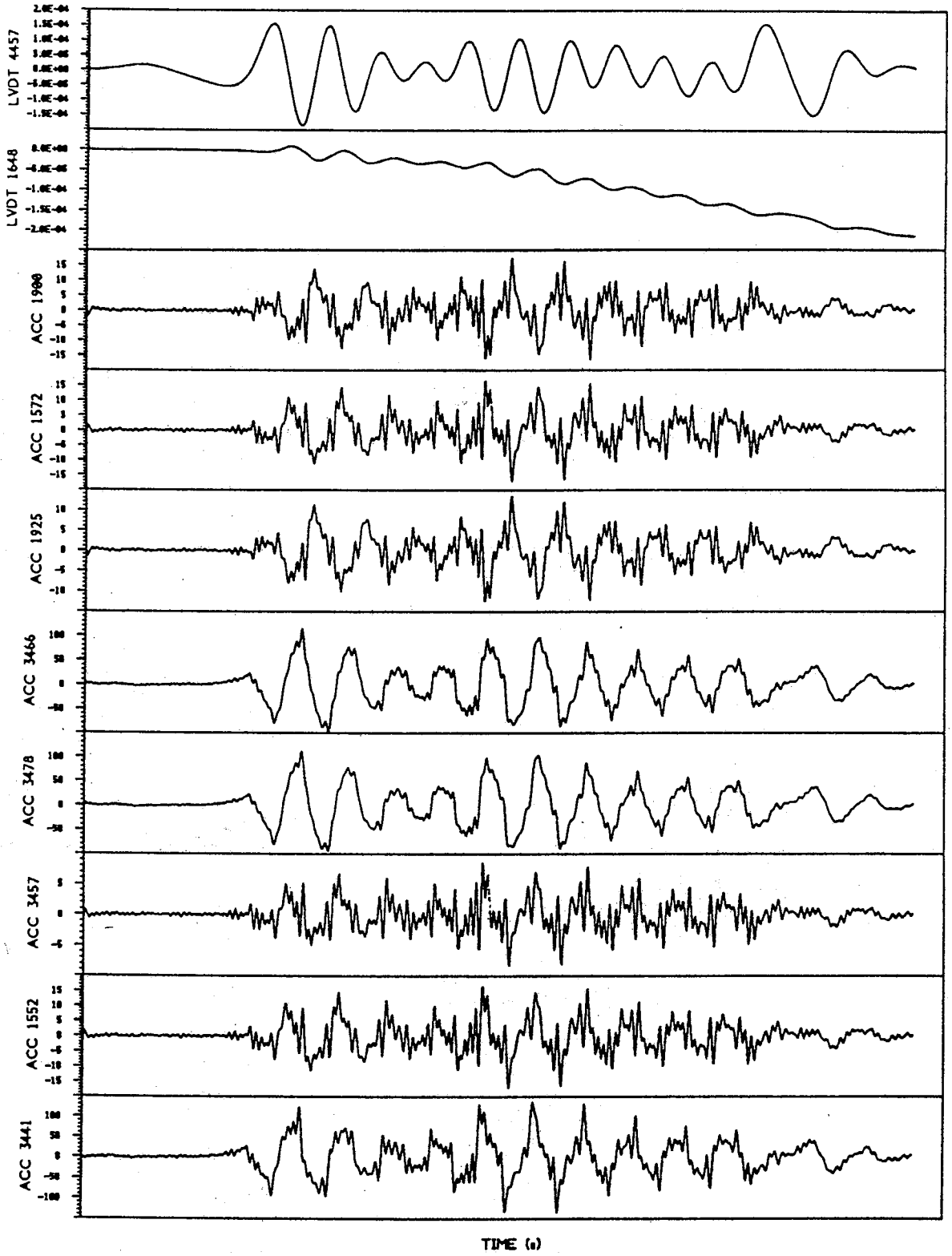

Fig. 6.26 Numerical analysis for Test RSS111 - EQ. NO: 5

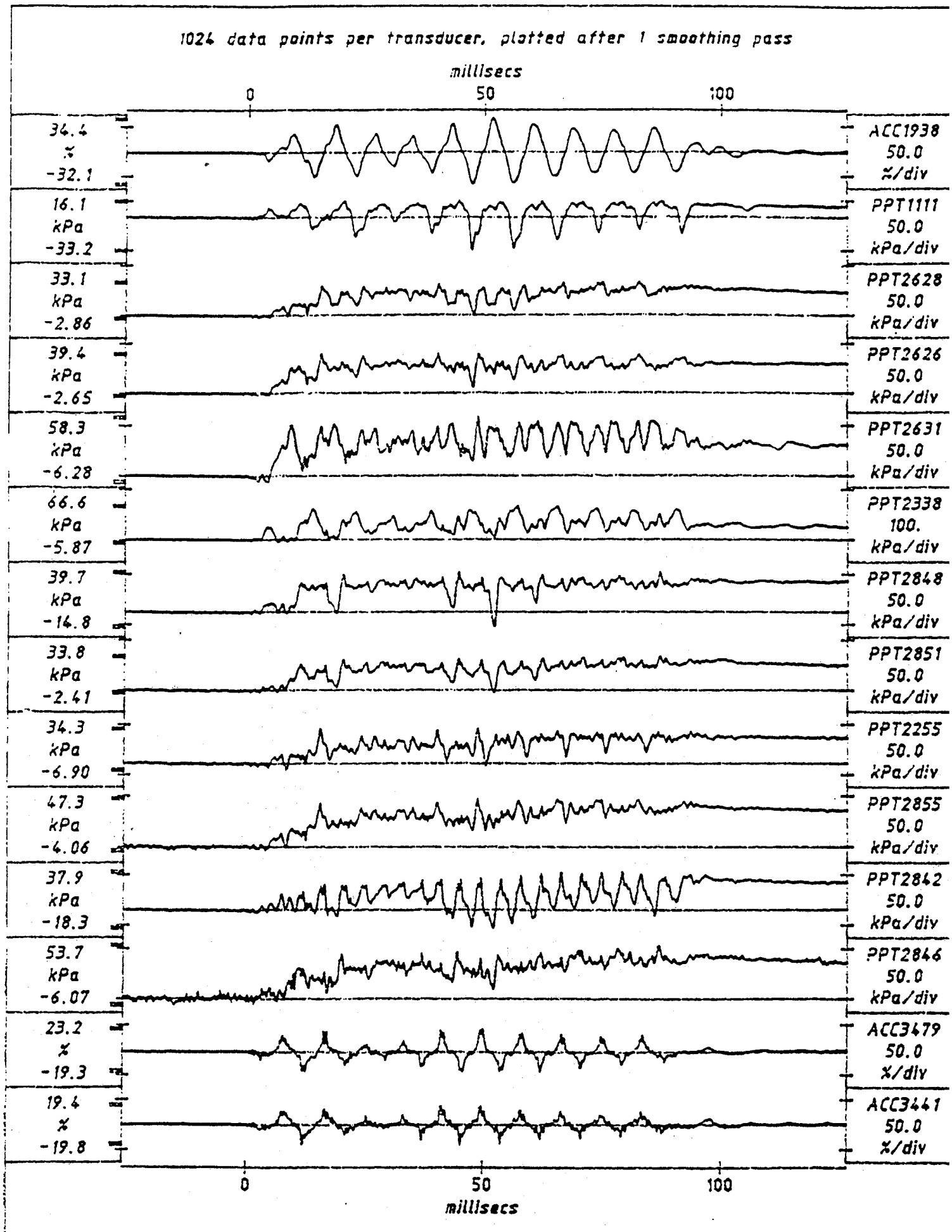

Scales : Model

TEST RSS111 MODEL SAT SURA F06	SHORT-TERM	G = 79.0g Km = 19.6%	FIG.NO.

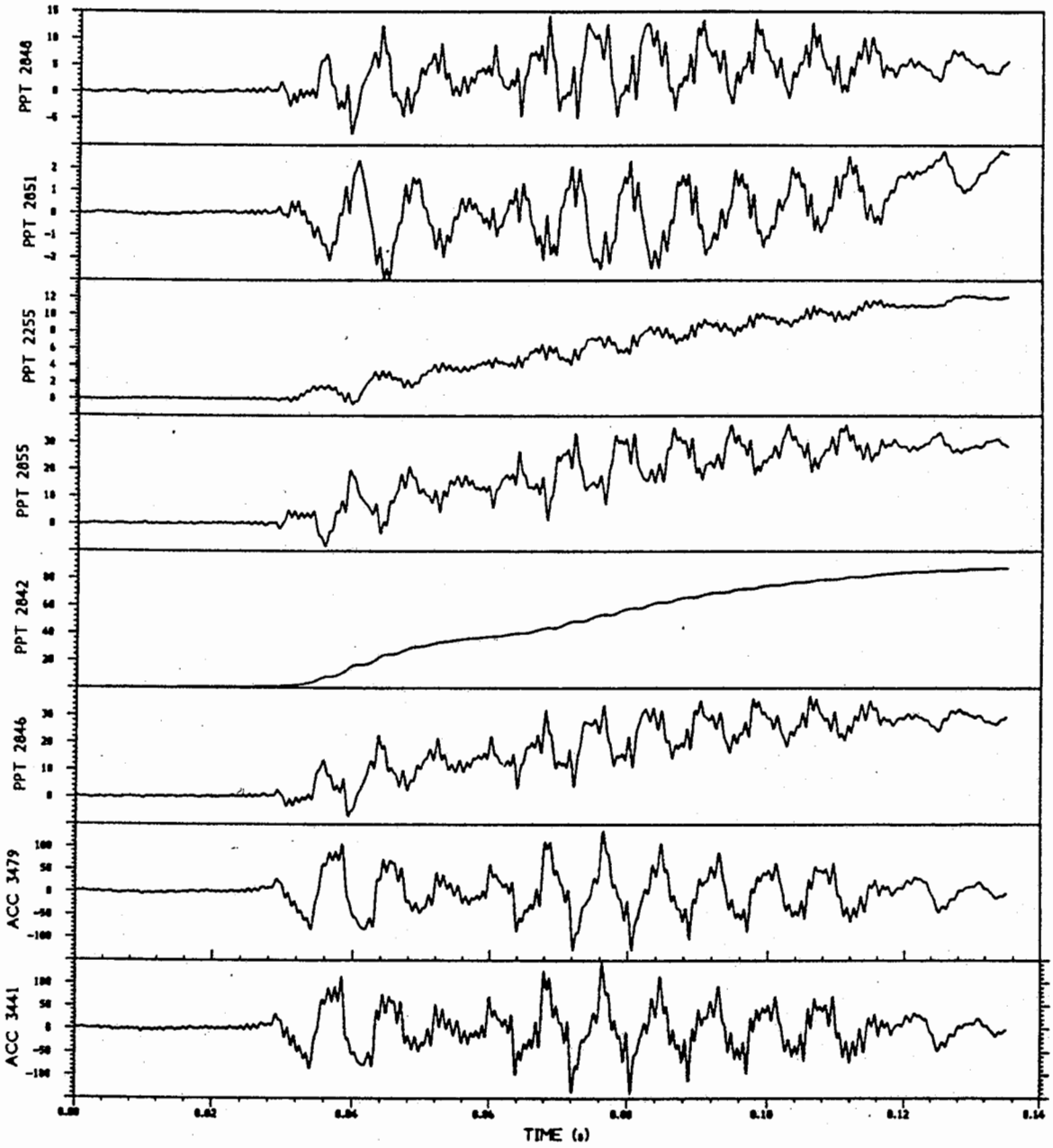

Fig. 6.28 Numerical analysis for Test RSS111 - EQ. NO: 6

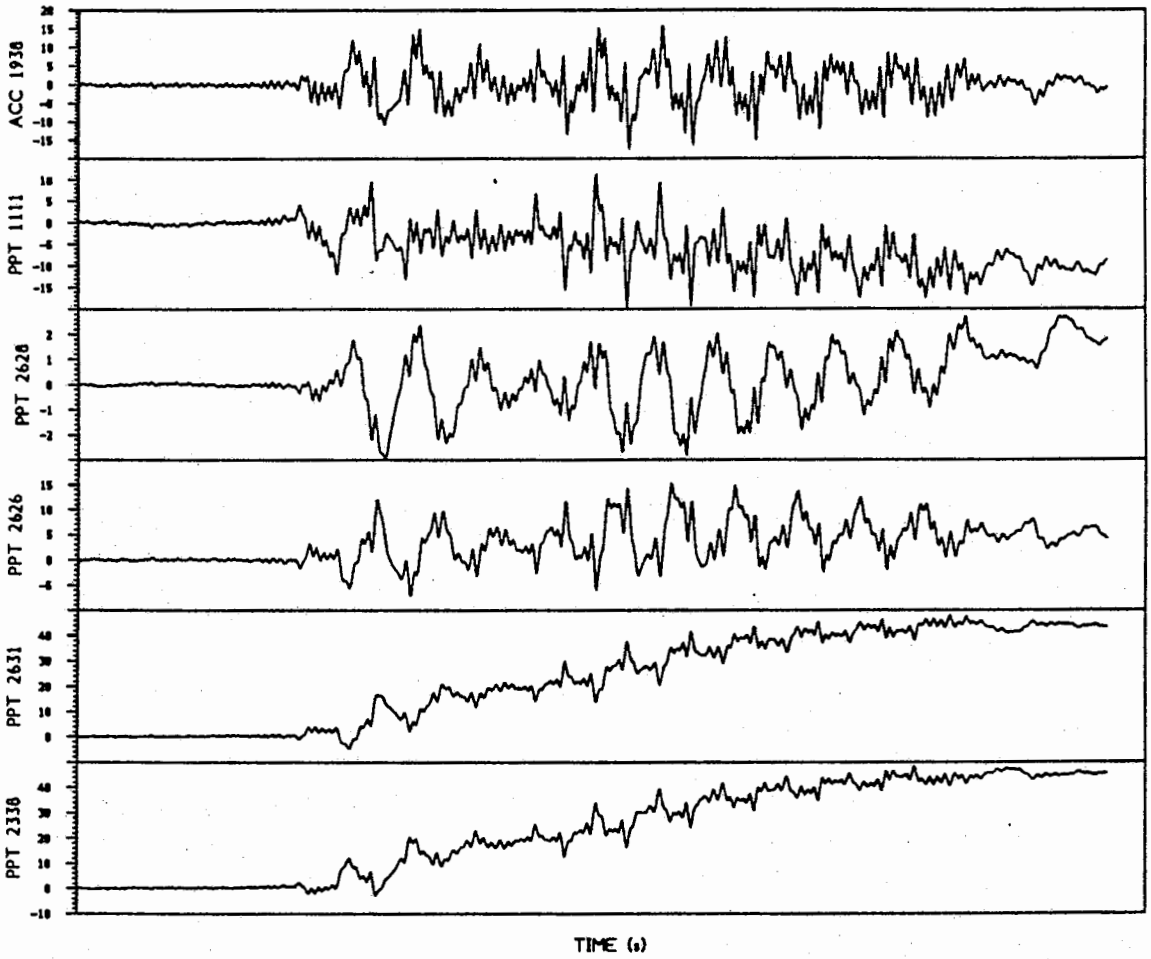

Fig. 6.28 Numerical analysis for Test RSS111 - EQ. NO: 6 (cont.)

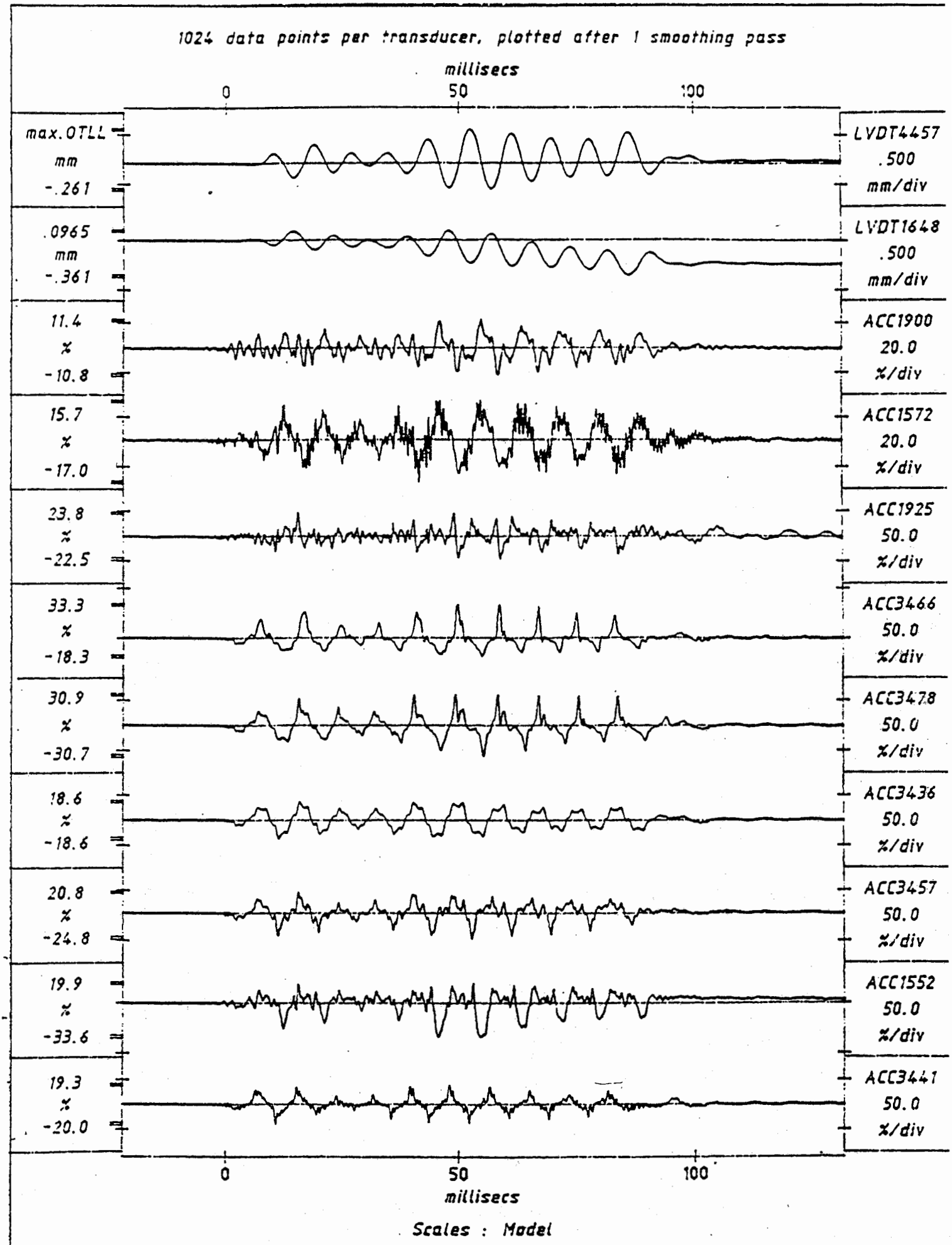

TEST RSS111 MODEL SAT SURB FLIGHT 1	EQ6	SHORT-TERM TIME RECORDS	G = 79.0g Km = 19.7% Kp = 20.0%	FIG. NO. 6.29

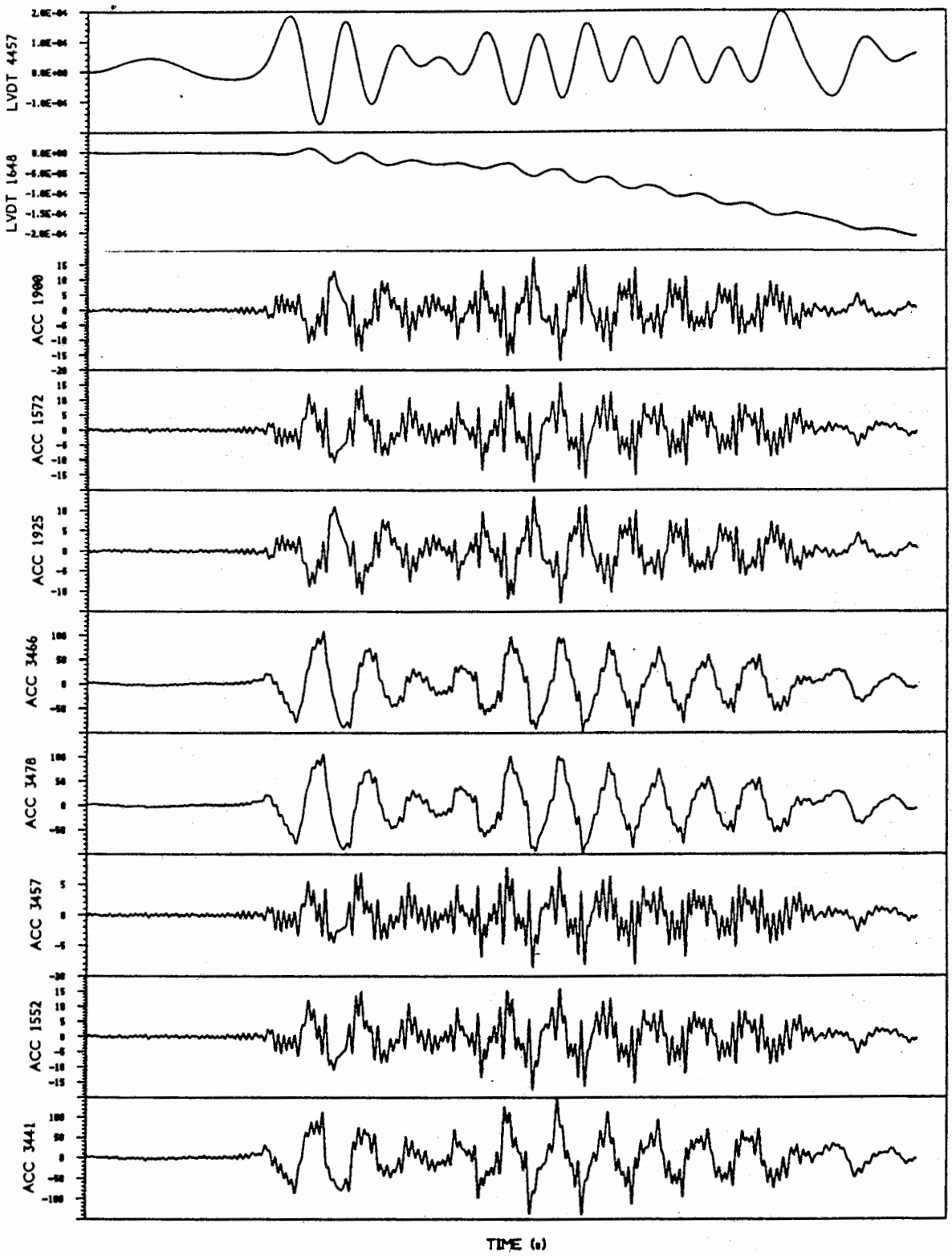

Fig. 6.30 Numerical analysis for Test RSS111 - EQ. NO: 6